Earth and Planetary Science Letters 492 (2018) 264–278

Contents lists available at ScienceDirect

Earth and Planetary Science Letters

www.elsevier.com/locate/epsl

Tropical Indo-Pacific hydroclimate response to North Atlantic forcing during the last deglaciation as recorded by a speleothem from Sumatra, Indonesia

Jennifer B. Wurtzel [a,b,*], Nerilie J. Abram [a,b], Sophie C. Lewis [b,c], Petra Bajo [d,e], John C. Hellstrom [d], Ulrike Troitzsch [a], David Heslop [a]

[a] Research School of Earth Sciences, Australian National University, Canberra, ACT, Australia
[b] ARC Centre of Excellence for Climate System Science, Australian National University, Canberra, ACT, Australia
[c] School of Physical Environmental and Mathematical Sciences, University of New South Wales, Canberra, ACT, Australia
[d] School of Earth Sciences, University of Melbourne, Melbourne, VIC, Australia
[e] School of Geography, University of Melbourne, Melbourne, VIC, Australia

ARTICLE INFO

Article history:
Received 12 May 2017
Received in revised form 14 March 2018
Accepted 1 April 2018
Available online 24 April 2018
Editor: H. Stoll

Keywords:
speleothem
oxygen isotopes
Indo-Pacific
Younger Dryas
ITCZ
deglaciation

ABSTRACT

Abrupt changes in Atlantic Meridional Overturning Circulation are known to have affected the strength of the Indian and Asian Monsoons during glacial and deglacial climate states. However, there is still much uncertainty around the hydroclimate response of the Indo-Pacific Warm Pool (IPWP) region to abrupt climate changes in the North Atlantic. Many studies suggest a mean southward shift in the intertropical convergence zone (ITCZ) in the IPWP region during phases of reduced Atlantic meridional overturning, however, existing proxies have seasonal biases and conflicting responses, making it difficult to determine the true extent of North Atlantic forcing in this climatically important region.

Here we present a precisely-dated, high-resolution record of eastern Indian Ocean hydroclimate variability spanning the last 16 ky (thousand years) from $\delta^{18}O$ measurements in an aragonite–calcite speleothem from central Sumatra. This represents the western-most speleothem record from the IPWP region. Precipitation arrives year-round at this site, with the majority sourced from the local tropical eastern Indian Ocean and two additional long-range seasonal sources associated with the boreal and austral summer monsoons. The Sumatran speleothem demonstrates a clear deglacial structure that includes ^{18}O enrichment during the Younger Dryas and ^{18}O depletion during the Bølling–Allerød, similar to the pattern seen in speleothems of the Asian and Indian monsoon realms. The speleothem $\delta^{18}O$ changes at this site are best explained by changes in rainfall amount and changes in the contributions from different moisture pathways. Reduced rainfall in Sumatra during the Younger Dryas is most likely driven by reductions in moisture transport along the northern or southern monsoon transport pathways to Sumatra. Considered with other regional proxies, the record from Sumatra suggests the response of the IPWP to North Atlantic freshwater forcing is not solely driven by southward shifts of the ITCZ, but also a reduction in moisture transport along both monsoon pathways.

1. Introduction

The last glacial termination was characterized by multiple millennial-scale shifts in global climate. Records of the last deglaciation from Greenland exhibit a sequence of abrupt climatic shifts, starting with the cold interval, Heinrich Stadial 1 (HS1, ~17.5–14.7 ka; thousand years ago) (Heinrich, 1988). This was followed by an abrupt warm event (the Bølling–Allerød (BA, ~14.7–12.9 ka)), a transition back to near glacial conditions during the Younger Dryas (YD; ~12.9–11.7 ka) that culminated in Holocene warmth starting ~10 ka (NGRIP members, 2004; Stuiver and Grootes, 2000).

Though the precise cause of abrupt cold events is still debated, there is strong evidence to suggest that they are related to the instability of large ice sheets during glacial terminations (Broecker et al., 2010; Denton et al., 2010). The YD and HS1 events have been identified in North Atlantic marine sediments as increases in ice-rafted debris associated with increased iceberg and meltwater discharge (Bond et al., 1993). The freshwater input into the North

* Corresponding author at: Research School of Earth Sciences, Australian National University, Canberra, ACT, Australia.
E-mail address: jennifer.wurtzel@anu.edu.au (J.B. Wurtzel).

https://doi.org/10.1016/j.epsl.2018.04.001
0012-821X/

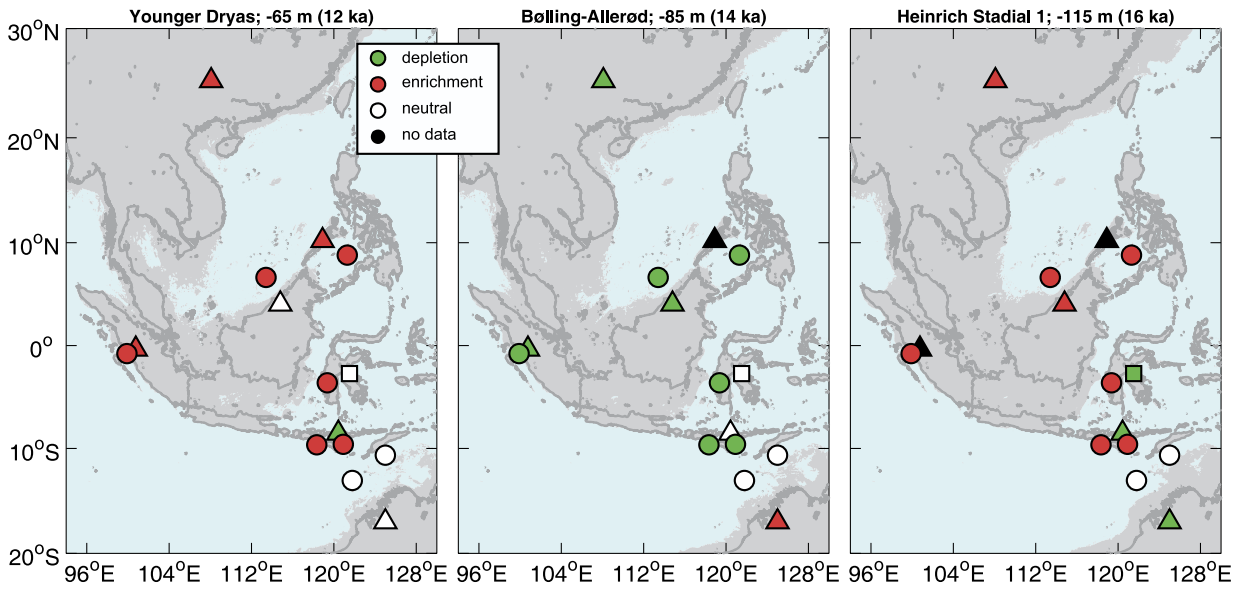

Fig. 1. Maps of IPWP proxies discussed in text for three intervals of interest: Heinrich Stadial 1 (16 ka), Bølling–Allerød (14 ka), and the Younger Dryas (12 ka). Marker shapes denote seawater $\delta^{18}O$ (circles), speleothem $\delta^{18}O$ (triangles), and leaf wax δD (square) and marker colors denote direction of the anomaly in terms of depletion of ^{18}O or D (green), enrichment of ^{18}O or D (red), neutral (white), and no data available for the interval (black). Anomalies are classified relative to the preceding interval (YD:BA, BA:HS1, HS1:LGM). The dark grey outline indicates modern coastline, while medium grey shading represents exposed shelf during periods of lower sea level. Sea level was inferred from the curve of Lambeck et al. (2014). (For interpretation of the colors in the figure(s), the reader is referred to the web version of this article.)

Atlantic severely weakened Atlantic Meridional Overturning Circulation (AMOC), reducing northward ocean heat transport, and cooling the Northern Hemisphere (McManus et al., 2004). In response, the Southern Hemisphere warmed during the cold stadials, HS1 and the YD, and warming stalled during the Antarctic Cold Reversal (ACR), the southern counterpart to the BA (Barker et al., 2009; Knutti et al., 2004). In response to this "bipolar seesaw", in which reorganization of ocean circulation during stadials redistributes heat from the Northern Hemisphere to the Southern Hemisphere, there is an accompanying reorganization of atmospheric circulation as the mean position of the Intertropical Convergence Zone (ITCZ) shifts southward (Chiang and Bitz, 2005; Zhang, 2005). This, in turn, drives the Southern Hemisphere westerlies southward, increases upwelling and CO_2 ventilation in the Southern Ocean, and feeds back into deglacial warming (Denton et al., 2010).

Proxy data from the Cariaco Basin show evidence for this mean southward movement of the ITCZ through a reduction in rainfall in the tropical Atlantic during the YD (Hughen et al., 1996). The Greenland deglacial sequence had far-reaching impacts on precipitation well beyond the North Atlantic. In the Asian and Indian Summer Monsoon realm, speleothem records from Dongge (Dykoski et al., 2005), Hulu (Wang et al., 2001), and Mawmluh Caves (Dutt et al., 2015) exhibit ^{18}O enrichment, interpreted as severely weakened monsoon intensity, during HS1 and the YD, and ^{18}O depletion (monsoon strengthening) during the BA (Fig. 1). Several mechanisms have been proposed to connect the North Atlantic to the Indian and Asian Monsoons. These include a stationary Rossby wave atmospheric teleconnection between the North Atlantic and India (Mohtadi et al., 2014), perturbations in the position of the Northern Hemisphere subtropical westerly jet (Marzin et al., 2013), and changes to the mean state of Pacific Walker circulation (Zhang and Delworth, 2005). Despite uncertainty about the teleconnection mechanism, abundant empirical evidence exists connecting climate changes in the tropical Indian Ocean region with the North Atlantic, and significant progress has been made towards understanding the regional manifestation of the YD in the Asian monsoon realm.

Both model (Pausata et al., 2011) and proxy (Tierney et al., 2015) data indicate that the regional response in the Indian Ocean to North Atlantic cold snaps is a cooling of western tropical Indian Ocean SSTs. The results of Pausata et al. (2011) suggest that changes in Indian Ocean SSTs during North Atlantic stadials is the primary contributor to changes in the Indian Monsoon with cooler Indian Ocean SSTs causing a reduction in precipitation transported over the Indian Ocean and Indian subcontinent. As a result, speleothem records of precipitation along this path (e.g., Mawmluh, Dongge, and Hulu Caves) exhibit either reduced rainfall during the YD and HS1, or isotopically enriched signals due to reduced rain-out along the transport path (or a combination of both).

Despite clear North Atlantic signals in Asian speleothems, the manifestation of high-latitude millennial-scale climate events in the Indo-Pacific Warm Pool remains a subject of ambiguity, due to the conflicting information on hydrological variability during the last termination interpreted from the limited number of high-resolution proxy records from this region. For example, speleothem $\delta^{18}O$ from Borneo (Partin et al., 2007) and leaf wax δD from Sulawesi (Konecky et al., 2016) show no response to the Younger Dryas or Bølling–Allerød (Fig. 1). However, seawater-$\delta^{18}O$ ($\delta^{18}O_{sw}$) estimates from the South China Sea (Steinke et al., 2006), Sulu Sea (Rosenthal et al., 2003), and Makassar Strait (Schröder et al., 2016) exhibit a deglacial pattern including the YD, BA, and HS1. In the southern IPWP, speleothems from Flores record ^{18}O depletion, suggesting an increase in rainfall during the YD and HS1 that has been interpreted as a mean southward shift of the ITCZ (Ayliffe et al., 2013; Griffiths et al., 2009). In contrast, two seawater-$\delta^{18}O$ reconstructions from just south of Flores suggest a reduction in rainfall during the YD and HS1 (Gibbons et al., 2014; Levi et al., 2007), while two more in the Timor Sea show no change (Stott et al., 2004; Xu et al., 2008). Furthermore, there is evidence to suggest that northern Australia received enhanced austral summer monsoon rainfall during HS1, and reduced rainfall during the BA, however the YD signal is unclear in these records (Denniston et al., 2013; Muller et al., 2008).

Cool SSTs in the tropical western Indian Ocean during cold stadials are not mirrored in the tropical eastern Indian Ocean (Mohtadi et al., 2014). Planktonic foraminiferal Mg/Ca-SST reconstructions from offshore West Sumatra show little temperature response to either the YD or HS1 (Mohtadi et al., 2014), simi-

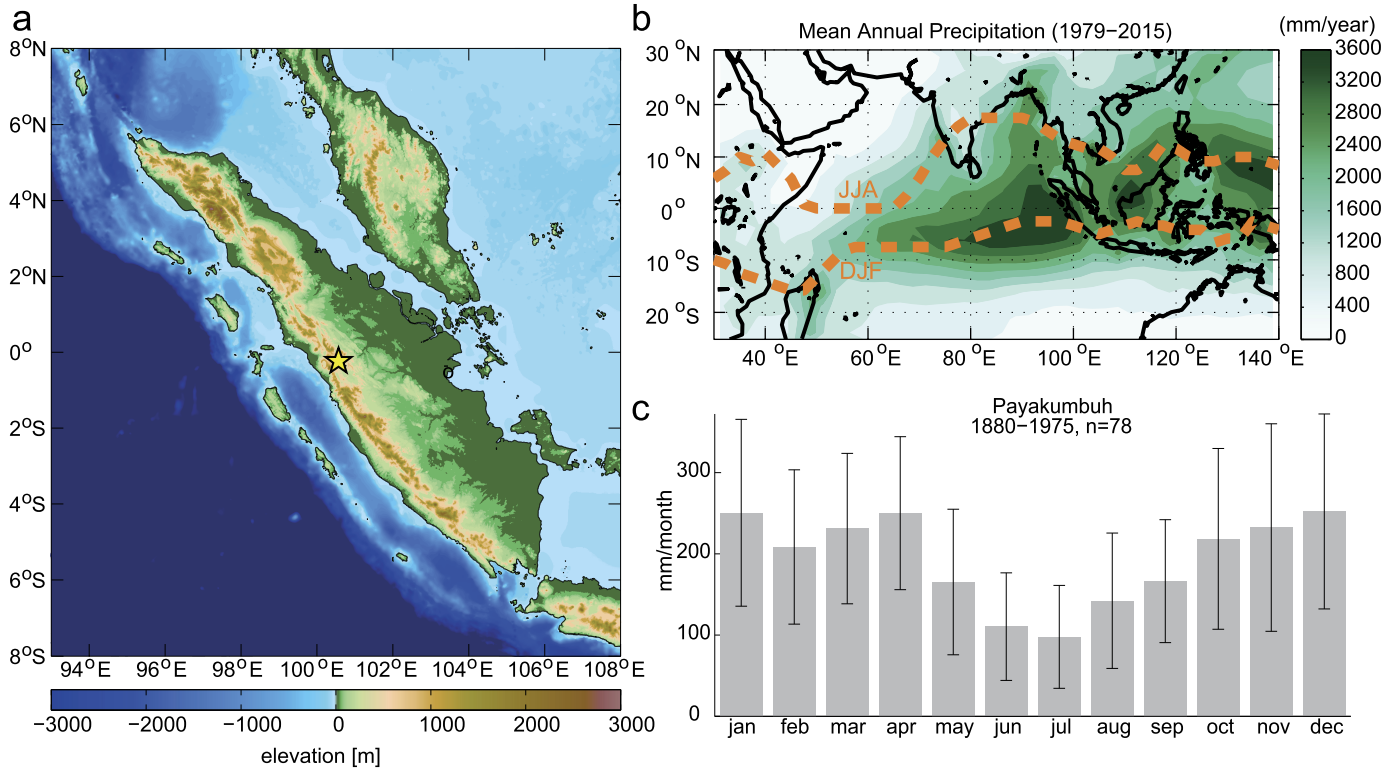

Fig. 2. (a) Topographic map of Sumatra with study site marked by star. (b) Mean annual precipitation (1979–2015) in the Indo-Pacific region from CPC Merged Analysis of Precipitation (Xie and Arkin, 1997). The position of maximum meridional rainfall (inferred from minimum outgoing longwave radiation; Liebmann and Smith, 1996) during JJA and DJF is indicated. (c) Mean monthly rainfall from Payakumbuh (∼20 km from cave site).

lar to other SST reconstructions from the IPWP (Gibbons et al., 2014). There is, however, a clear hydrologic change seen in the seawater oxygen isotope reconstruction from the same site. The $\delta^{18}O_{sw}$ records a strong increase (decrease) during the YD and HS1 (BA), interpreted by the authors as a change in local salinity due to reduced (increased) rainfall, which they attribute to reorganization of Hadley circulation in the Indian Ocean (Mohtadi et al., 2014).

Because the IPWP lies at the intersection between numerous hydrological climate phenomena that have widespread zonal (Walker circulation) and meridional (Hadley circulation, ITCZ, Australasian monsoon) ramifications, it is important to gain a clearer understanding of how this region responded to abrupt climate changes in the past. In light of disparities between IPWP reconstructions of the last deglacial, it is prudent to consider both marine and terrestrial proxies, as well as consider seasonality and meridional-zonal controls on hydrologic variability. Here we present a deglacial-Holocene rainfall record spanning 16,500 yrs from a precisely-dated, decadally-resolved aragonite–calcite stalagmite from central West Sumatra. This is the first speleothem record from the Indian Ocean sector of the IPWP, and the westernmost for all IPWP speleothem sites. The cave site is located ∼100 km from sediment core SO189-39KL, and provides a complementary terrestrial perspective to the marine reconstruction. We compare our record to other hydroclimate records in the Asian and Indian Summer Monsoon (ASM/ISM) realms and in the Indo-Pacific Warm Pool region. We use these results to examine spatial and seasonal differences in Asia and Indo-Pacific Warm Pool hydroclimate during the Bølling–Allerød and Younger Dryas periods. We additionally compare a detailed modern climatology with results from a general circulation model equipped with vapor source distribution (VSD) tracers to infer which moisture sources may be driving precipitation changes under hosing conditions.

2. Study site and climatology

Tangga Cave (0°21′S, 100°45′E, 600 m) is located in the Barisan Mountains of central West Sumatra, Indonesia (Fig. 2). The caves here are in carbonate host rocks formed in the mid-Miocene (Wilson, 2002).

2.1. Modern climatology

Modern climatology at Tangga Cave was calculated using meteorological data from a nearby (∼20 km) weather station in Payakumbuh village (−0.22°N, 100.62°E) that was active between 1880–1941 and 1951–1975 (Peterson and Vose, 1997). No stations within 100 km were in operation after 1975. Average annual rainfall exceeds 2000 mm yr $^{-1}$ (Fig. 2). Rain is received throughout the year, but with a relative minimum in June–July–August. Using NOAA's Hybrid Single Particle Lagrangian Integrated Trajectory (HYSPLIT4) model with the NCEP/NCAR Reanalysis V2 gridded dataset, we analyzed daily back trajectories of rain-bearing air masses to our study site from January 2000 to December 2010 (Draxler and Hess, 1997). Cluster analysis of the 6-day back trajectories of rainfall events (>8.5 mm/day) identifies three primary sources of rainfall delivered to Tangga Cave (Fig. 3a). Approximately 69% of average annual rainfall is sourced from the equatorial eastern Indian Ocean (59% local, 10% distal), and arrives throughout the year. From late-April through mid-November, rainfall can also be sourced from the Timor Sea, and this accounts for 17% of the annual average. These trajectories are associated with the southeasterly trades that form during the boreal summer monsoon. From late November through mid-March, this SE trade wind source is cut off and replaced by a long-range South China Sea source. These northeasterly trajectories are associated with circulation patterns of the austral summer monsoon, and contribute 9% of the average annual rainfall to Tangga Cave. Approximately 5%

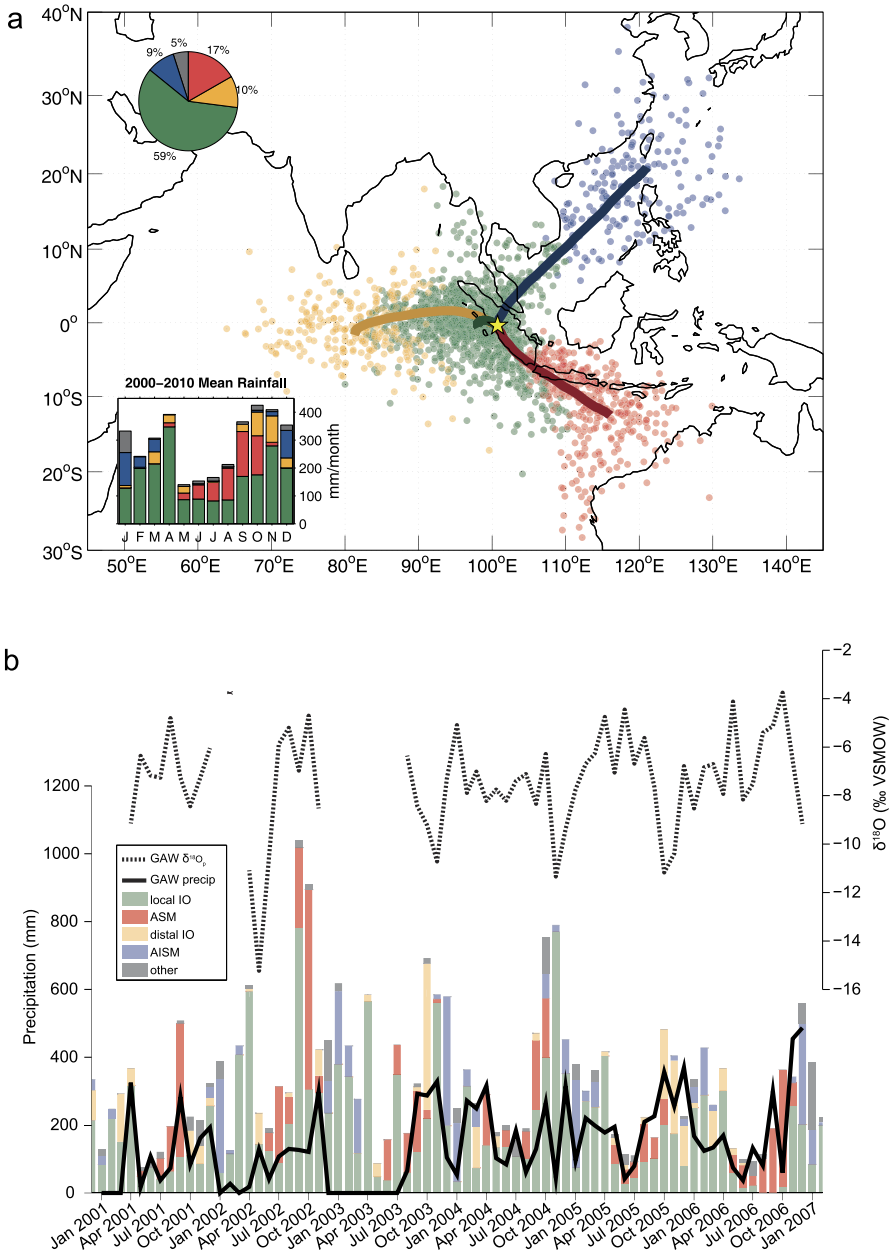

Fig. 3. (a) Four primary paths of source moisture to Tangga Cave. Paths were generated using cluster analysis of rain-bearing 6-day back-trajectories over 2000–2010 period. Red, blue, yellow and green lines indicate results of HYSPLIT trajectory cluster analysis, with pie chart representing % annual rainfall from each of those sources. Grey represents unassigned trajectories. Inset shows mean monthly rainfall over the analysis period at Tangga Cave from ERA-interim 0.7° gridded data (Dee et al., 2011) with colors corresponding to source cluster. Colored dots represent starting points of all rain-bearing 6-day back trajectories corresponding to cluster. (b) HYSPLIT monthly source contributions for 2001–2006 using ERA-interim precipitation data. Color coding is the same as in Fig. 3a. Black lines are precipitation amount (solid) and precipitation $\delta^{18}O$ (dashed) from Kototabang (GAW) station (0.12°S, 100.19°E, 865 m).

of annual rainfall does not fall into the 3 major trajectory clusters. The cluster contributions show excellent agreement with an earlier study using seven tagged Indo-Pacific water source regions in a single-layer, Rayleigh-type, isotope-enabled GCM (Suwarman et al., 2013). These results corroborate previous studies that suggest rainfall variability in western and northern Sumatra is not dominated by monsoon seasonality (Aldrian and Susanto, 2003; Mohtadi et al., 2014).

2.2. Controls on rainfall $\delta^{18}O$ at Tangga Cave

Regional rainfall stations with isotope data demonstrate that Indonesian rainfall can be described by four groups based on seasonal isotopic variability (Belgaman et al., 2017). These four rainfall types correspond to the rainfall regions as defined by Aldrian and Susanto (2003). Rainfall in central Sumatra has similar isotopic characteristics to northern Sumatra and western Borneo, consisting of two peaks each year of high $\delta^{18}O$ related to seasonal migration of the ITCZ. Rainfall $\delta^{18}O$ in this domain tends to show only a weak amount effect (Belgaman et al., 2017).

Drip and rainwater monitoring were not feasible at the cave site in this study. However, limited monthly rainfall isotope data is available from nearby station, Kototabang (100.19°E, 0.12°S, 865 masl, GAW), spanning the interval from February 2001 to January 2007 and consisting of 59 rainfall $\delta^{18}O$ observations (Kurita et al., 2009). Analysis of Kototabang station data over this period shows that ~24% of isotopic variance is explained by the local amount effect at 95% significance (Suwarman et al., 2013). However, multiple

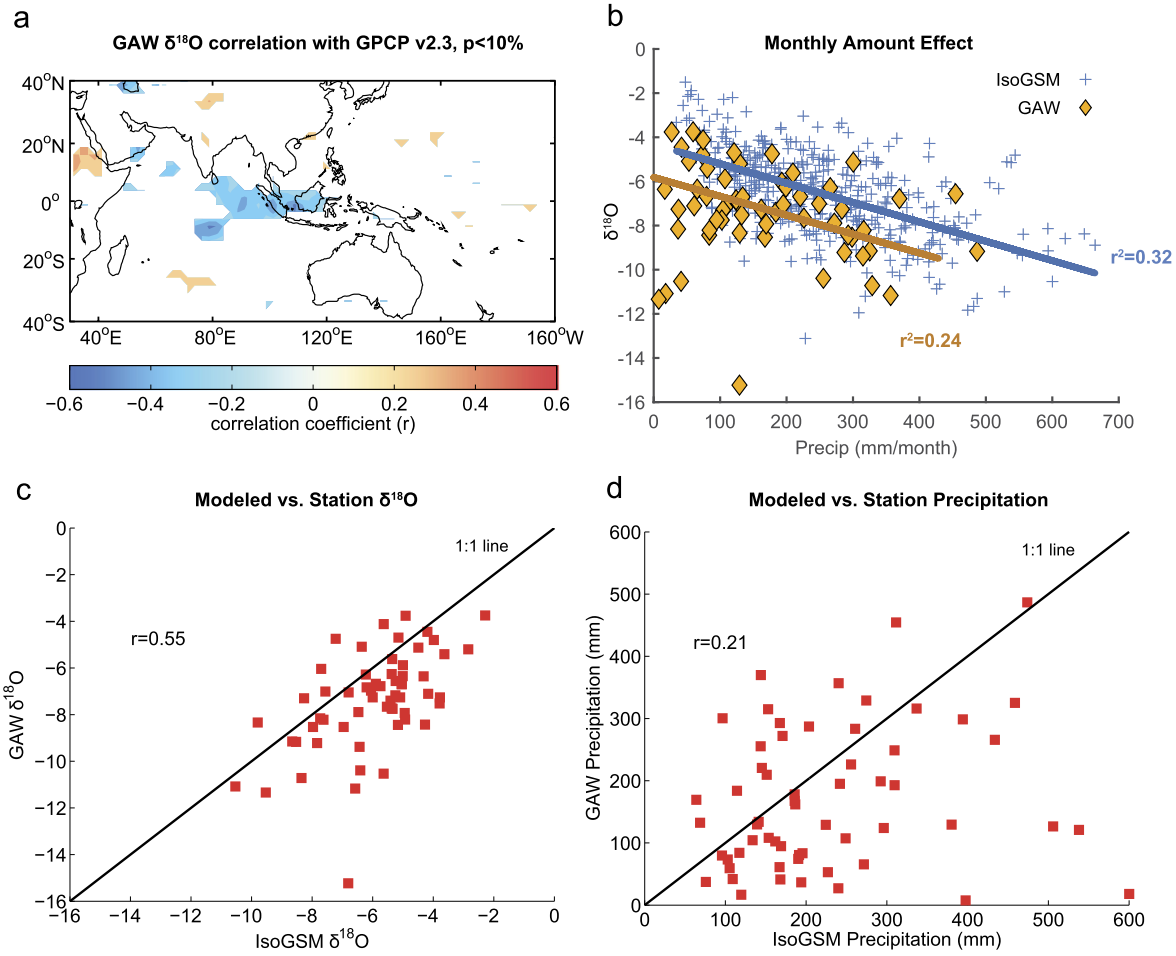

Fig. 4. (a) Map showing the correlation coefficient of Kototabang (GAW) station precipitation $\delta^{18}O$ with mean annual precipitation from GPCP v2.3 over the period 2001–2006. Colors represent r-values significant at 90% level. (b) Linear regression between IsoGSM simulated monthly precipitation amount and simulated monthly precipitation $\delta^{18}O$ (blue crosses) at grid point closest to Tangga Cave (1979–2013), and linear regression between GAW precipitation amount and monthly $\delta^{18}O$ (orange diamonds), demonstrating amount effect. (c) Correlation between observed monthly precipitation $\delta^{18}O$ (GAW) and simulated monthly precipitation $\delta^{18}O$ (IsoGSM) for the period 2001–2006. (d) Correlation between observed monthly precipitation amount (GAW) and simulated precipitation amount (IsoGSM) for months with rainfall >0 mm for the period 2001–2006.

studies have demonstrated that the contribution of the amount effect is stronger on longer time-scales (Kurita et al., 2009; Moerman et al., 2013) and when considering larger regions (the "regional amount effect") (Moerman et al., 2013). Correlation of Kototabang $\delta^{18}O$ with GPCP v2.3 precipitation shows that a similar relationship ($r = -0.4$ to -0.5) exists over a broader region of the eastern Indian Ocean (Fig. 4a).

For the purpose of examining the modern relationship of precipitation $\delta^{18}O$ to rainfall at the study site over a longer time interval, we use existing output from the spectrally nudged, isotope-enabled general circulation model, IsoGSM (Yoshimura et al., 2008). Previous studies have shown that IsoGSM data correlates well with GNIP station data in the ASM/ISM monsoon region (Sinha et al., 2015; Yang et al., 2016). IsoGSM data from the $1.8 \times 1.9°$ grid point nearest Tangga Cave demonstrates that up to 32% of the variance in isotopic values of annual average rainfall on interannual timescales is controlled by the local amount effect, compared to the 24% predicted by Kototabang station (Fig. 4b). There is a strong correlation between station and modeled oxygen isotope data ($r = 0.55$; Fig. 4c) over the period of overlap; however, the correlation between station and modeled precipitation data is very weak ($r = 0.21$; Fig. 4d). The low correlation between observed and simulated precipitation likely stems from highly spatially variable rainfall over the mountain ranges of Sumatra; there may be significant differences in local amount between Kototabang and the study site, which is averaged in the IsoGSM grid box. The strong correlation that exists in the isotope data is further evidence that the isotopes are regionally coherent, even if rainfall amount is not.

Previous modeling studies using tagged moisture source suggest that Asian summer monsoon rainfall is subject to less rainout during transport than Indian Ocean rainfall, despite a longer transport pathway, causing ASM rainfall arriving at the site to be relatively enriched in ^{18}O (Belgaman et al., 2016; Suwarman et al., 2013). Conversely, Indian Ocean moisture transport is subject to greater condensation along its path, producing more negative $\delta^{18}O$ at the site. On a seasonal scale, these moisture source characteristics should enhance the amount effect. In austral winter (June–August; JJA), there is a higher proportion of enriched ASM rainfall arriving at Tangga Cave. Additionally, less average rainfall during JJA should contribute to the more positive $\delta^{18}O$ signal. Conversely, during transition seasons when the ITCZ is overhead (March–May and September–November; MAM and SON), there is increased rainfall and a higher proportion of Indian Ocean sources, both of which should contribute to lighter $\delta^{18}O$.

To assess the combined influence of moisture source with amount effect, we compared the Kototabang precipitation and isotope time series with changes in contributions from HYSPLIT-derived sources over the same time period (Fig. 3b). This analysis highlights the dominance of the local Indian Ocean moisture source throughout the year. Three large ^{18}O depletion events

(April–May 2002, October–November 2003, October–November 2005) occur during spring/autumn when rainfall is generally high and when Indian Ocean contributions (local and distal) are highest, supporting the idea that moisture source and amount effect act in the same direction. Surprisingly, the largest rainfall event (September–October 2002) is associated with relatively enriched values; however, this may be as a result of the above-average proportion of enriched ASM rainfall offsetting the amount effect. It appears then that while negative δ^{18}O excursions tend to be associated with increased rainfall, increased rainfall does not necessarily produce a negative δ^{18}O excursion. Heavier δ^{18}O values are generally associated with an increase in ASM rainfall sources. In particular, the heaviest values occur during September–October 2006 when local Indian Ocean sources were replaced solely by ASM sources as a result of a strong Indian Ocean Dipole event (Abram et al., 2008).

This analysis, along with the broader correlation of Kototabang isotopes with eastern Indian Ocean rainfall amount, suggests that the local eastern Indian Ocean source is the dominant driver of isotopic depletion in rainfall δ^{18}O at the cave site, both through changes in amount of rainfall being derived from this source and through changes in proportion of this source through time.

Modern seawater oxygen isotope data demonstrates less than a 0.1‰ variation between the three trajectory source regions (LeGrande and Schmidt, 2006). Estimates of LGM seawater isotopic anomalies suggest that the South China Sea may have been relatively depleted by up to 0.3‰ or enriched up to 0.4‰ and the Indian Ocean and Timor Seas may have been enriched by up to 0.5‰ relative to present (Waelbroeck et al., 2014). Assuming a constant fractionation factor over a constant distance over time, there is a maximum 0.5‰ change related to moisture source composition from a single source. With respect to the isotope variability recorded by the Tangga Cave record since the LGM (see Section 4), these values are relatively small. Likewise, the effect of mixing these two moisture sources at a given time in the past, though dependent on the mixing proportion, is limited to the maximum anomaly of +0.5‰, and could be less if the enriched and depleted source averaged out. Therefore, we do not expect source moisture composition changes to be a primary contributor to changes in the speleothem isotope record. Based on the analyses presented here and regional coherence with other speleothem records, we interpret speleothem δ^{18}O at the cave site as an annually integrated signal of rainfall amount (dominated by eastern Indian Ocean contributions) as well as the combined influence of multiple moisture transport paths with varying isotopic compositions.

3. Materials and methods

3.1. Speleothem sampling

The entrance to Tangga Cave is at the base of a sinkhole covered with jungle vegetation. The cave narrows considerably ~50 m from the entrance, and descends steeply to a lower level with an underground river passage. The main sample used in this study, TA12-2, was collected from a small chamber located ~105 m from the cave entrance. The specimen was found in a toppled position on a muddy substrate in the lower level of the cave (but above the river).

TA12-2 was slabbed and hand polished before sampling (Fig. 5). The total length is ~50 cm with a relatively constant diameter of ~4 cm. TA12-2 is visibly laminated with alternating light and dark layers for the top 38 cm. Between 38–44 cm, it is comprised of white needle-like crystalline material, and the final section from 44–50 cm has similar laminations to the upper section.

The central slab was sampled continuously for stable isotope analysis at 0.5 mm resolution along its central growth axis using a micromill with a 1 mm diameter mill bit. Powders for U-series sampling were collected adjacent to the isotope transect. The offcut slab that faced the milled slab surface was hand-broken (to avoid losing material by sawing) into seven pieces less than 9.5 cm length. These pieces were used for used for laser ablation inductively coupled plasma mass spectrometer (ICP-MS) trace element analysis and Raman spectroscopy. After laser analysis, these pieces were used to create petrographic thin sections along the entire length of the specimen.

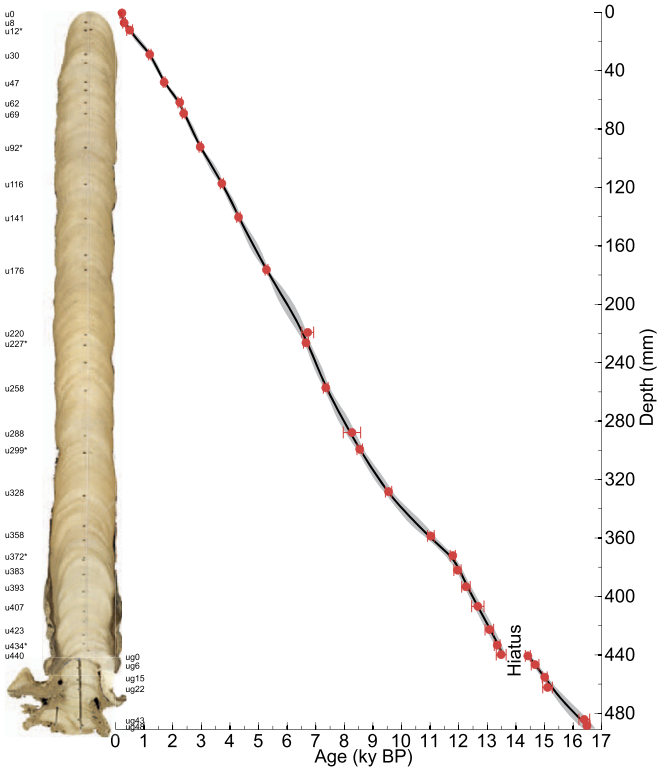

Fig. 5. Image of TA12-2 next to U/Th age-depth model for TA12-2. Red circles with 2σ error indicate where dates were taken. Black line is age-depth model. 2σ confidence interval is marked in grey. Age model and uncertainties generated in Bacon software for R (Blaauw and Christen, 2011). Groove on image shows milling transect for δ^{18}O samples. Holes beside milling transect show locations where powders were collected for U/Th analysis (Note: not all powders analyzed). *Dates generated at RSES, ANU.

3.2. Mineralogical determination

TA12-2 was initially screened for mineralogy using XRD at two points along the specimen, which indicated an aragonitic composition. However, subsequent detailed trace element analysis indicated that some layers are instead composed of calcite. The techniques described below were used to determine mineralogy along the length of the specimen.

3.2.1. Laser ablation ICP-MS trace element analysis

Trace element measurements were made at the Australian National University using an ArF Excimer laser ablation system (193 nm; Lambda Physik LPX120i) coupled with a single collector Varian 820 quadrupole inductively coupled plasma mass spectrometer (ICP-MS). All sample tracks were pre-ablated using a 265 µm spot size at 10 Hz moving at 200 µm/s in order to pre-clean the trace element analysis track. Analyses were conducted by pulsing the laser at 5 Hz with a 40 µm round ablation spot moving at 40 µm/s. Twenty elemental masses (^{11}B, ^{23}Na, ^{24}Mg, ^{25}Mg, ^{27}Al, ^{31}P, ^{43}Ca, ^{44}Ca, ^{47}Ti, ^{55}Mn, ^{66}Zn, ^{86}Sr, ^{88}Sr, ^{89}Y, ^{137}Ba, ^{138}Ba, ^{139}La, ^{208}Pb, ^{232}Th, ^{238}U) were measured for transects running along

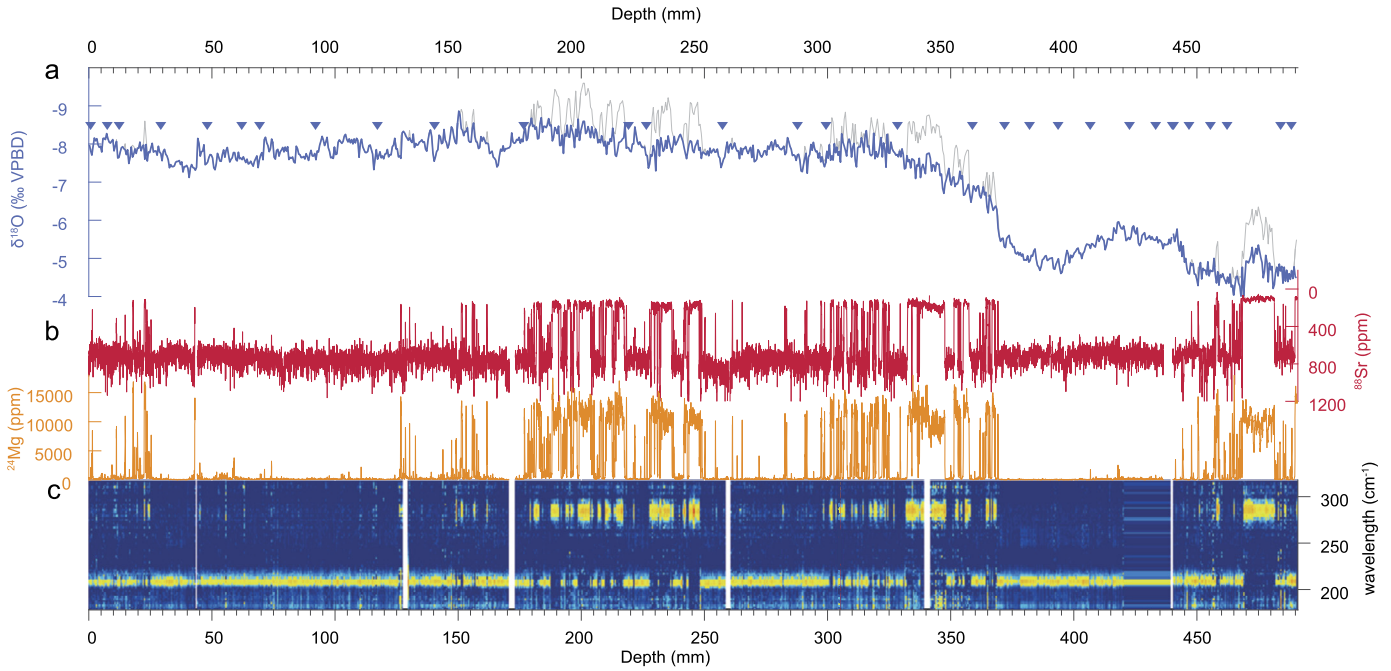

Fig. 6. Mineral identification and oxygen isotope correction. Depth vs. a) raw speleothem $\delta^{18}O$ (grey) corrected to aragonite values using 1‰ offset (blue), b) strontium (red) in ppm plotted on reversed *y*-axis and magnesium (orange) in ppm plotted on log-scale, d) Raman power spectra showing diagnostic wavelength bands for calcite (280 cm^{1}) and aragonite (206 cm^{1}). Antiphased behavior in the trace elements and power in the Raman calcite band correspond to anomalous depletions in the oxygen isotope record relative to aragonite values. Aragonite layers were targeted for U/Th date samples (blue triangles).

the growth axis of TA12-2. Analysis was also performed on three standards (NIST612, NIST610, in-house coral NEP 3B) and for background counts. The standards and background were measured before and after each analysis transect to correct for drift. All data was corrected relative to the NIST612 glass standard, and normalized to ^{43}Ca, using a MATLAB script written by the author. Calcite and aragonite phases are evident in the Sr and Mg content of the speleothem.

3.2.2. Raman spectroscopy

Raman spectroscopy is a non-destructive method that can be used to identify the relative amounts of mineral phases using the vibrational modes of different crystal lattices. In the case of carbonate, the different crystal structures of aragonite and calcite produce distinct Raman spectra, despite sharing the same $CaCO_3$ composition (White, 2006). Raman analysis was performed along the same analysis track as the trace element laser ablation analysis. Raman analysis was carried out at the ANU's Research School of Physics on a Renishaw InVin Raman spectrometer, using a 632 nm red laser at 50% power with 1200 mm^{-1} grating. A 20× objective lens with a 1.93 µm diameter spot size was used in conjunction with a 1 second acquisition time. Spectra were collected in a broad spectral frequency range from 120–1974 cm^{-1}, but the low frequency range between 150–300 cm^{-1} was used for identifying the diagnostic peaks for calcite (280 cm^{-1}) and aragonite (206 cm^{-1}).

3.2.3. Thin section petrography

Thin sections were created from the same offcut slab pieces used for trace element analysis. These pieces were further reduced in size to create a full 13-piece transect of 2x1″ thin sections. The unpolished thin sections were prepared at the ANU and photographed at high magnification using a Leica Power Mosaic at the RSES. Thin sections were used to verify the mineralogical classifications derived from trace element and analysis and Raman spectroscopy. Further analysis and identification of mineralogy and diagenetic features was performed at the School of Environmental and Life Sciences at the University of Newcastle. Mineralogical analysis of the thin section samples will be discussed in a subsequent publication, and for the purposes of this manuscript are only used as additional verification of aragonite–calcite phases identified by trace element and Raman spectroscopy methods.

3.2.4. Mineralogy

High-resolution laser ablation ICP-MS trace element analysis revealed abrupt anti-phased shifts in magnesium and strontium of several orders of magnitude (Fig. 6). Magnesium and strontium are known to be preferentially incorporated into calcite and aragonite lattices, respectively (Finch et al., 2001). As such, the distinct shifts in TA12-2 speleothem trace element composition are indicative of alternating layers of aragonite and calcite. The sample is predominantly aragonite, but abrupt excursions to high Mg (low Sr) composition are indicative of calcite layers in the speleothem.

This interpretation is supported by Raman analysis, which definitively identifies the two $CaCO_3$ polymorphs. Raman spectroscopy reveals TA12-2 to be primarily composed of aragonite with irregular intervals of calcite deposition mainly occurring between 180–250 mm depth, 280–370 mm depth, and 460–470 mm depth. Thin section petrography further confirms that these calcite layers precipitated as primary material and that the sample as a whole has undergone only minor secondary micro-replacement to calcite (Silvia Frisia, pers. comm.). This retention of the primary mineralogical phases is critical to the interpretation of the Tangga climate record, as recrystallization of aragonite to calcite can result in the loss of the original $\delta^{18}O$ signal and loss of uranium (Bajo et al., 2016). U/Th dating results obtained from two different laboratories are in good agreement (Table 1). This consistency as well as the stratigraphic sequence of all 31 dates support the notion that even if TA12-2 experienced minor U-loss, it is highly likely that chronology presented in this study is accurate and representative of primary depositional conditions.

Table 1
U/Th data for stalagmite TA12-2.

Sample ID	Depth (mm)	^{238}U (ppm) $\pm 2\sigma$	[^{230}Th/^{232}Th]	[^{230}Th/^{238}U]	[^{234}U/^{238}U]	Uncorrected age[a] (ky BP)	Corrected age[a] (ky BP)	Corr. initial [^{234}U/^{238}U]
u0	0.7	0.985 ± 0.075	1.7	0.0057 ± 0.0006	1.5176 ± 0.0099	0.345 ± 0.043	0.2223 ± 0.0658	1.5180 ± 0.0099
u8	7.4	15.999 ± 1.250	2.4	0.0064 ± 0.0004	1.5197 ± 0.0182	0.395 ± 0.029	0.3000 ± 0.0481	1.5202 ± 0.0183
u12[b]	12.4	10.087 ± 0.009	7.6	0.0083 ± 0.0004	1.5234 ± 0.0018	0.531 ± 0.029	0.4936 ± 0.1015	1.5242 ± 0.0018
u30	29.1	9.641 ± 0.770	13.5	0.0183 ± 0.0005	1.5289 ± 0.0096	1.247 ± 0.037	1.1988 ± 0.0417	1.5308 ± 0.0096
u47	48.0	8.906 ± 0.704	27.1	0.0246 ± 0.0004	1.5056 ± 0.0117	1.730 ± 0.033	1.6971 ± 0.0349	1.5081 ± 0.0117
u62	61.9	8.823 ± 0.751	12.7	0.0333 ± 0.0007	1.5254 ± 0.0095	2.339 ± 0.053	2.2452 ± 0.0651	1.5288 ± 0.0095
u69	69.4	7.968 ± 0.636	30.1	0.0342 ± 0.0006	1.5146 ± 0.0105	2.422 ± 0.048	2.3820 ± 0.0501	1.5182 ± 0.0105
u92[b]	92.3	8.818 ± 0.008	54.4	0.0420 ± 0.0005	1.5208 ± 0.0023	2.984 ± 0.037	2.9587 ± 0.0410	1.5253 ± 0.0023
u116	117.4	9.852 ± 0.782	9.1	0.0518 ± 0.0006	1.5095 ± 0.0101	3.736 ± 0.052	3.7153 ± 0.0524	1.5149 ± 0.0102
u141	140.4	9.983 ± 0.784	49.8	0.0597 ± 0.0006	1.5047 ± 0.0118	4.340 ± 0.057	4.2971 ± 0.0595	1.5110 ± 0.0119
u176	176.4	10.366 ± 0.909	38.6	0.0735 ± 0.0005	1.5142 ± 0.0029	5.347 ± 0.039	5.2786 ± 0.0477	1.5220 ± 0.0029
u220	219.3	9.719 ± 1.777	46.9	0.0920 ± 0.0026	1.5052 ± 0.0096	6.789 ± 0.204	6.7194 ± 0.2067	1.5150 ± 0.0097
u227[b]	226.4	9.313 ± 0.012	201.5	0.0906 ± 0.0011	1.5079 ± 0.0020	6.669 ± 0.084	6.6555 ± 0.0850	1.5176 ± 0.0020
u258	257.2	11.764 ± 0.936	117.6	0.0998 ± 0.0009	1.5071 ± 0.0085	7.379 ± 0.082	7.3487 ± 0.0829	1.5178 ± 0.0086
u288	287.8	10.044 ± 1.465	7.5	0.1175 ± 0.0025	1.4930 ± 0.0073	8.836 ± 0.203	8.2664 ± 0.3038	1.5047 ± 0.0075
u299[b]	299.3	10.860 ± 0.011	80.4	0.1153 ± 0.0012	1.5051 ± 0.0014	8.589 ± 0.094	8.5399 ± 0.0966	1.5175 ± 0.0014
u328	328.3	13.034 ± 1.022	61.8	0.1274 ± 0.0012	1.4921 ± 0.0069	9.622 ± 0.106	9.5475 ± 0.1097	1.5056 ± 0.0070
u358	358.6	16.017 ± 1.323	139.9	0.1448 ± 0.0012	1.4879 ± 0.0080	11.040 ± 0.116	11.0263 ± 0.1153	1.5034 ± 0.0082
u372[b]	372.1	12.924 ± 0.008	1339.0	0.1552 ± 0.0011	1.4978 ± 0.0020	11.794 ± 0.090	11.7922 ± 0.0897	1.5147 ± 0.0020
u383	382.0	10.943 ± 0.855	822.1	0.1572 ± 0.0013	1.4968 ± 0.0080	11.964 ± 0.125	11.9564 ± 0.1258	1.5139 ± 0.0082
u393	393.4	10.943 ± 0.847	194.6	0.1605 ± 0.0016	1.4908 ± 0.0083	12.282 ± 0.149	12.2523 ± 0.1491	1.5081 ± 0.0085
u407	406.8	10.683 ± 0.894	678.7	0.1649 ± 0.0025	1.4866 ± 0.0081	12.677 ± 0.215	12.6682 ± 0.2166	1.5044 ± 0.0083
u423	422.7	10.570 ± 0.846	498.9	0.1704 ± 0.0016	1.4912 ± 0.0080	13.083 ± 0.151	13.0699 ± 0.1501	1.5097 ± 0.0082
u434[b]	433.3	16.166 ± 0.012	1195.4	0.1732 ± 0.0012	1.4873 ± 0.0021	13.348 ± 0.101	13.3452 ± 0.1003	1.5061 ± 0.0021
u440	439.9	15.786 ± 1.331	23.9	0.1769 ± 0.0013	1.4768 ± 0.0081	13.756 ± 0.134	13.4856 ± 0.1718	1.4954 ± 0.0083
ug0	0	19.579 ± 1.571	66.1	0.1831 ± 0.0013	1.4532 ± 0.0030	14.520 ± 0.075	14.4174 ± 0.0855	1.4721 ± 0.0031
ug6	6.5	13.368 ± 1.019	177.7	0.1859 ± 0.0012	1.4577 ± 0.0078	14.709 ± 0.132	14.6710 ± 0.1330	1.4771 ± 0.0080
ug15	15.1	17.353 ± 1.424	98.4	0.1891 ± 0.0009	1.4489 ± 0.0026	15.079 ± 0.082	15.0061 ± 0.0865	1.4682 ± 0.0027
ug22	22.1	18.569 ± 1.481	213.1	0.1898 ± 0.0017	1.4487 ± 0.0076	15.141 ± 0.168	15.1078 ± 0.1697	1.4683 ± 0.0078
ug43	44.0	17.043 ± 1.351	61.0	0.2057 ± 0.0018	1.4478 ± 0.0073	16.517 ± 0.180	16.3920 ± 0.1866	1.4691 ± 0.0075
ug48	48.2	17.727 ± 1.483	57.5	0.2073 ± 0.0009	1.4505 ± 0.0029	16.622 ± 0.086	16.4869 ± 0.1013	1.4720 ± 0.0030

[a] Age in ky BP; thousands of years before present where present is defined as 1950 A.D. Ages are calculated using decay constants specified in Cheng et al. (2013). All ratios [bracketed] are reported as activities. The uncertainty is reported as 2σ error. Corrected ages use an initial [^{230}Th/^{232}Th] of 0.5 ± 0.2 for the detrital component.
[b] Samples run at RSES.

3.3. Geochronology

Age control for the TA12-2 sample is based on thirty-one uranium–thorium (U/Th) dates. Aragonite layers were targeted for dating due to their high uranium concentrations (>10 ppm), and powders of 2–6 mg were used. Six dates were generated at the ANU on a Thermo Finnigan Neptune Plus multi-collector ICP-MS using the methods described in McCulloch and Mortimer (2008). Twenty-five dates were generated at the University of Melbourne on a Nu Instruments Plasma multi-collector ICP-MS using the methods of Hellstrom (2003).

The U–Th dating results are summarized in Table 1. Ages are given in thousands of years before present (ky BP; where "present" is defined as 1950 A.D.). All 31 U-series dates for TA12-2 fall in stratigraphic order within error. For all but the top sample, uranium concentrations exceeded 8 ppm, due to the high incorporation of uranium into the aragonite lattice. There was significant variation in the ^{230}Th/^{232}Th measurements ranging from 1.7 to 1339.

Ages were corrected for the initial ^{230}Th concentration using the stratigraphical constraint model of Hellstrom (2006), an initial [^{230}Th/^{232}Th] of 0.5 ± 0.2 and the U and Th decay constants of Cheng et al. (2013). Ages were calculated and corrected for initial [^{230}Th/^{232}Th] in MATLAB using Monte Carlo simulations ($n = 10^4$) to account for 2σ uncertainties in each of the input variables and to determine errors on the resulting ages (Hellstrom, 2003; Scroxton, 2014). A hiatus occurs at a depth of 440 mm and spans ~0.88 ky between 13.5 ± 0.11 ky BP and 14.4 ± 0.10 ky BP (Fig. 5). The depth-age model for the speleothem was constructed separately for above and below the unconformity using a Bayesian Monte Carlo approach with the statistical software package, Bacon, for R (Blaauw and Christen, 2011) Results from Bacon compared well with the model using methods from (Hellstrom, 2006) but allowed more flexibility in dealing with the hiatus.

3.4. Stable isotope analysis

3.4.1. Analytical methods

Measurements of δ^{18}O were made on aliquots of milled powder weighing between 110 and 140 µg at the Australian National University using a Finnigan MAT-253 Isotope Ratio Mass Spectrometer coupled with an automated Kiel IV Carbonate device using 105% H_3PO_4 at 75 °C for carbonate reactions. Results are corrected using international standards NBS-19 ($\delta^{18}O = -2.20‰$ VPDB) and NBS-18 ($\delta^{18}O = -23.00‰$ VPDB; note: To maintain long-term consistency of δ^{18}O results from the RSES stable isotope facility, the old value of NBS-18 δ^{18}O composition is used). The internal standard of ANU-M2 ($\delta^{18}O = -7.32‰$) was also routinely analyzed as an additional data quality monitor. The analytical error for measurements of NBS-19 and ANU-M2 were calculated by finding the standard deviation across all runs. Using this method, the analytical error was 0.041‰ ($n = 144$, 1σ) for NBS-19 δ^{18}O, and 0.070‰ ($n = 44$, 1σ) for ANU-M2 δ^{18}O. Stable isotope values are expressed in delta notation (δ) as per mille (‰) deviations, relative to Vienna Peedee Belemnite (VPDB). The oxygen isotope profile for TA12-2 is based on 901 isotopic measurements.

3.4.2. Isotopic corrections

The carbonate deposition in aragonite and calcite phases of the speleothem appears to be primary and so it is assumed that both polymorphs retain their original isotopic signals. This results in a relative depletion of ^{18}O in the calcite layers compared to

aragonite, due to the different isotopic fractionation coefficients of oxygen between the two phases. This offset has been previously quantified in synthetic aragonite and *in situ* mineralogical studies to be between 0.6–1.0‰ at 25 °C (Frisia et al., 2002; Kim et al., 2007).

Calcite layers in TA12-2 were defined using a 3-component Gaussian Mixture Model (GMM) (McLachlan and Peel, 2004) on the Mg–Sr laser ablation ICP-MS data set, consisting of ~18,000 data points. The optimal GMM identified a calcite component based on a high Mg–low Sr composition. All points within this cluster were assigned as calcite and all remaining points received an aragonite assignment. The laser ablation data was then binned according to stable isotope sample depth. On average, there are about 20 laser ablation measurements per stable isotope sample. Each isotope measurement was corrected to aragonite-equivalent isotopic values based on the fraction of calcite in the corresponding trace element bin, with a maximum offset of +1‰ for a bin containing 100% calcite composition. The use of this 1‰ mineralogical correction consistently brings the $\delta^{18}O$ values of calcite layers into agreement with the $\delta^{18}O$ of adjacent aragonite values.

In addition to mineralogical effects on the TA12-2 speleothem $\delta^{18}O$, the isotopic signal originally derives from marine-sourced rainfall and is therefore subject to effects from ice volume changes in ocean $\delta^{18}O$ over glacial–interglacial time-scales. Following the approach used in other studies (Carolin et al., 2013) all of the oxygen isotope records discussed in this paper (Figs. 7–8) are corrected for estimated changes in ice volume using the global sea water $\delta^{18}O$ curve developed by Bintanja et al. (2005). The only exception is the marine record, which was corrected using the Waelbroeck sea level curve by the original authors (Mohtadi et al., 2014). These corrections allow for interpretation of local salinity and rainfall changes without the additional isotopic component related to sea level (ice volume) changes over glacial–interglacial time scales.

4. Results and discussion

4.1. Speleothem $\delta^{18}O$ record

The 0.5 mm isotope sample resolution of TA12-2 is equivalent to a 15-yr sample resolution on average. The oldest part of the speleothem record (~16.5 ka) is characterized by relatively heavy values (~−5.2‰). The first prominent feature in the record is a negative excursion of ~1‰ centered around 15.8 ky BP. This is followed by an abrupt 1‰ shift at 14.7 ky BP to lighter oxygen isotope values, which corresponds to the onset of the Bølling–Allerød period. A short hiatus interrupts the record at 14.4 ky BP but growth resumes at 13.5 ky BP at near-similar isotopic values. This hiatus occurs where a natural break developed in the specimen after collection, and it is not clear if it represents a true cessation of growth or the absence of sampled material from this period due to a slight difference in the orientation of the speleothem slabs. The largest anomaly in the record begins at 13 ky BP and lasts until 11.5 ky BP with oxygen isotope values rising by 1.5‰ to a maximum of −5.1‰. Recovery occurs abruptly as isotope values decrease by 1.1‰ within 200 yrs. This anomaly corresponds remarkably well with the Younger Dryas event. Subsequent to the YD, values decrease more gradually over the next 2000 yrs, until they reach an average Holocene value of −8.0‰ ± 0.58‰.

4.2. Indian Ocean region

The Tangga Cave record shows many similarities to records of the Asian and Indian summer monsoons (ASM/ISM) during the last deglaciation. In particular, the Sumatran rainfall record demonstrates a clear response to North Atlantic millennial-scale events,

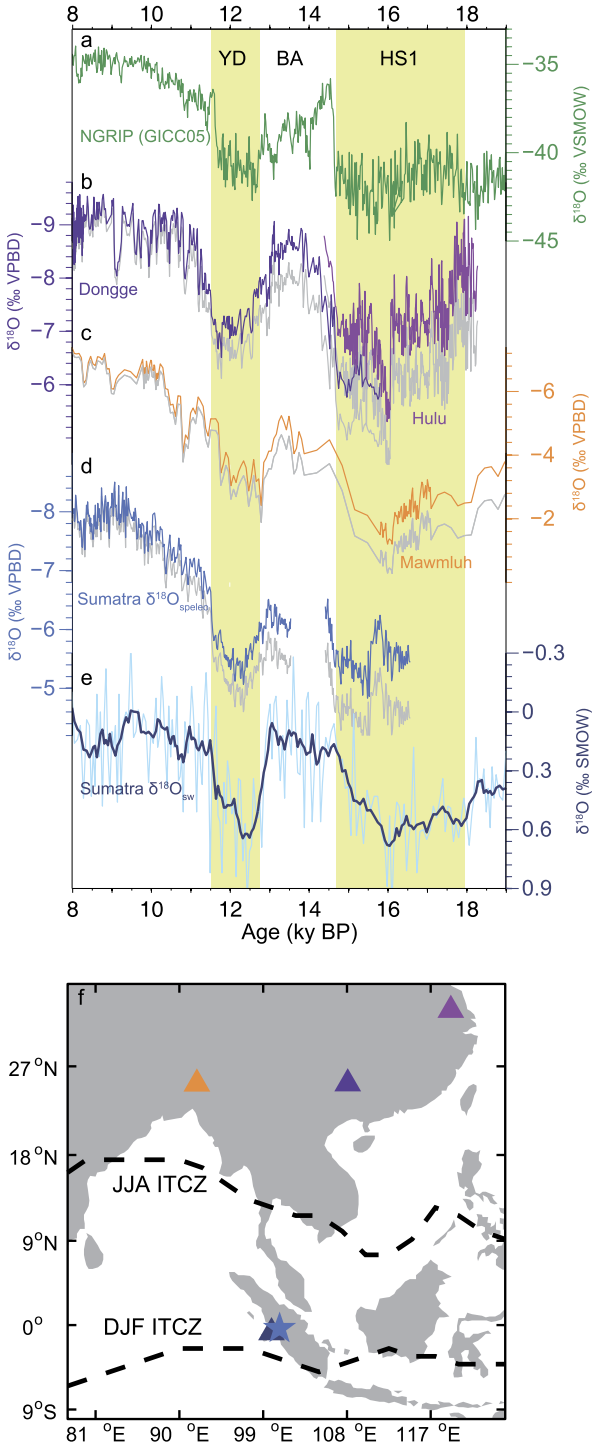

Fig. 7. Sumatra speleothem $\delta^{18}O$ over last deglaciation compared with other paleoclimate records. a) Greenland (NGRIP) ice core $\delta^{18}O$ with GICC05 chronology (NGRIP members, 2004; Vinther et al., 2006; Rasmussen et al., 2006) indicative of northern hemisphere high latitude temperature. b) Speleothem $\delta^{18}O$ from Dongge and Hulu Caves in China (Dykoski et al., 2005; Wang et al., 2001) and c) speleothem $\delta^{18}O$ from Mawmluh Cave in India (Dutt et al., 2015) reflecting Asian and Indian summer monsoon strength, respectively. d) Speleothem $\delta^{18}O$ from Tangga Cave in Sumatra (this study) and e) seawater $\delta^{18}O$ from SO189-39KL from offshore Sumatra in the eastern Indian Ocean (light blue) with 7-point running average (dark blue; Mohtadi et al., 2014). The speleothem and marine records have been adjusted for ice volume-related changes in global seawater $\delta^{18}O$ (Bintanja et al., 2005) following method of Carolin et al., 2013. Vertical shading denotes timing of YD and HS1. f) Location of records shown in a–e. Colors of symbols correspond to colors of time-series in a–e. The position of the modern maximum meridional rainfall in JJA and DJF is indicated by the dashed line.

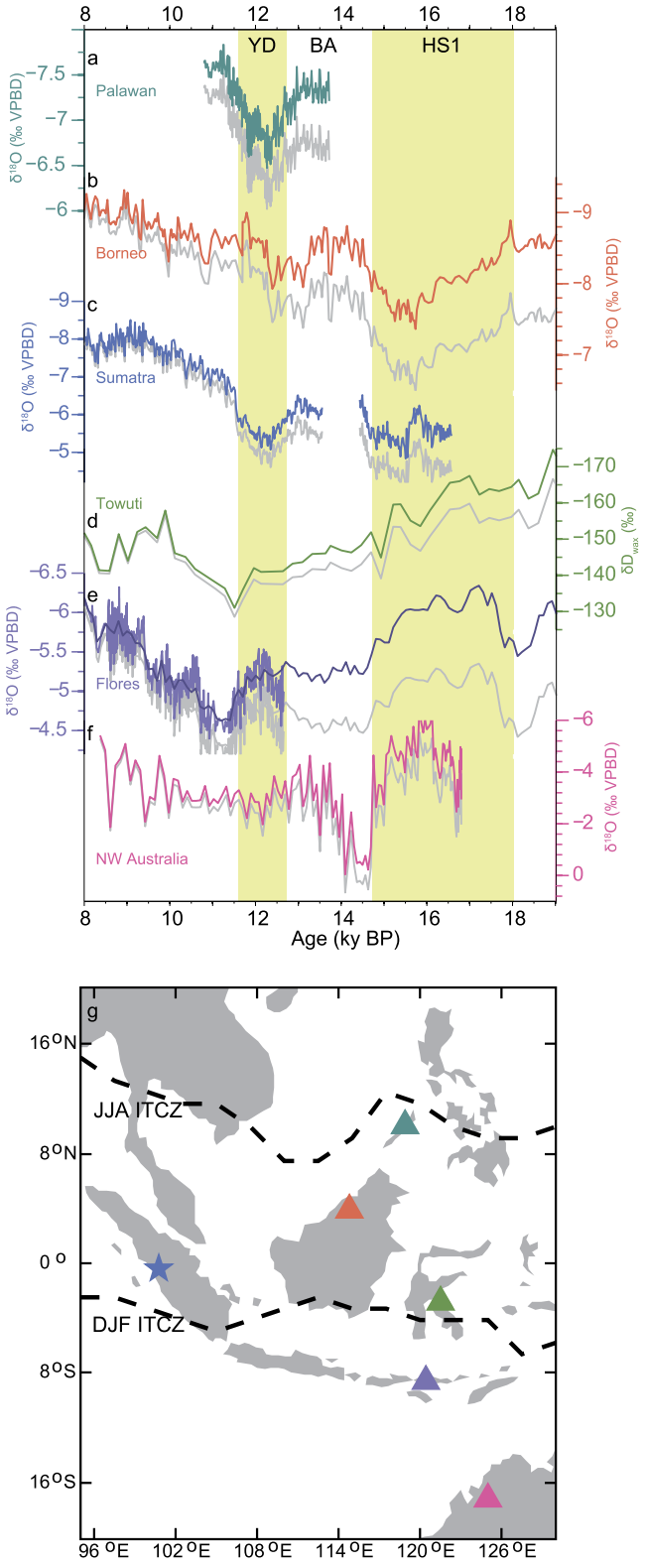

Fig. 8. The YD and BA climate events in proxies from the IPWP. From North to South, a) Palawan, Philippines (Partin et al., 2015); b) Gunung Buda, Borneo (Partin et al., 2007); c) Tangga Cave, Sumatra (this study); d) Lake Towuti, Sulawesi (Konecky et al., 2016); e) Liang Luar Cave, Flores (Griffiths et al., 2009); and f) Ball Gown Cave, Australia (Denniston et al., 2013). Vertical shading denotes timing of YD and HS1. g) Location of records shown in a–f. Colors of symbols correspond to colors of time-series in a–f. The position of the modern maximum meridional rainfall in JJA and DJF is indicated by the dashed line.

including distinct ^{18}O enrichment during the YD and depletion during the BA periods (Fig. 7). These features are consistent in sign and timing to those recorded in the NGRIP ice core temperature record and cave records of the Asian and Indian summer monsoon regions (Dutt et al., 2015; Dykoski et al., 2005; NGRIP members, 2004; Wang et al., 2001) (Fig. 7). As discussed earlier, the manifestation of North Atlantic events into India and Asia is well-established in many speleothem records (Dutt et al., 2015; Dykoski et al., 2005; Liu et al., 2013; Shakun et al., 2007; Wang et al., 2001). Their occurrence is thought to be related to a reduction of moisture transport from a cooler western Indian Ocean following a westerly transport path across the Indian Ocean and up through the Bay of Bengal onto the Asian continent (Liu et al., 2014).

The new speleothem record from Sumatra provides evidence that the ASM/ISM deglacial pattern also extended into the tropical eastern Indian Ocean. Though Tangga Cave $\delta^{18}O$ variability has complex influences from both amount effect and competing moisture sources, the regional coherence between multiple paleoclimate records suggests broad-scale mechanisms are in play. Comparison between the abrupt deglacial events in the Sumatran speleothem $\delta^{18}O$ record and the nearby marine sediment $\delta^{18}O_{sw}$ reconstruction (SO189-39KL; Mohtadi et al., 2014) shows excellent correspondence in the timing of the BA and YD events, including an extremely rapid termination of the YD. Other marine sediment studies from the eastern Indian Ocean that exhibit a robust BA-YD sequence are located in the Bay of Bengal and Andaman Sea. These sites are strongly influenced by the ISM, which provides a direct link to reduced runoff in boreal summer months during weak monsoon events associated with North Atlantic stadial events (Marzin et al., 2013; Sijinkumar et al., 2016).

Unlike these more northerly sites, the equatorial region offshore of Sumatra receives rainfall year-round with the boreal summer monsoon contributing to only a small portion (<25%) of the annual rainfall. This raises the question of why the equatorial eastern Indian Ocean records the YD-BA signal so prominently? Indeed, the work of (Sijinkumar et al., 2016) seems to indicate weaker structure of deglacial climate anomalies along an equator-ward (southward) transect in the Bay of Bengal (though it is noted that this southward attenuation of signal could be related to lower sedimentation rates and bioturbation). However, both the Sumatran speleothem and sediment core records carry a robust expression of the YD and BA climate events.

It has previously been suggested that ocean advection may play a role in the expression of the YD in the Sumatran seawater $\delta^{18}O$ history (Partin et al., 2015), however, the similarities between SO189-39KL and speleothem TA12-2 suggest an atmospheric hydroclimate signal, either via a local amount effect or a shared rainfall $\delta^{18}O$ integration history.

Isotopic values in Tangga Cave during the YD are similar to those preceding the BA, as is observed in the marine core. In contrast, the YD at Dongge and Mawmluh Caves are slightly lighter than values during HS1. Though interrupted by a growth hiatus, the onset, duration and termination of the BA are clear in the Tangga Cave speleothem, indicating a relative depletion of ^{18}O during this interval. The magnitude of the BA $\delta^{18}O$ signal at Tangga Cave is smaller relative to those in other speleothems from the ASM/ISM realm, which reach Holocene levels of isotopic depletion. The speleothem response is also smaller in magnitude than that of the adjacent marine core. As the speleothem likely records local hydrology, it is possible that the amplified BA isotopic signal in the marine core is a result of advection of continental runoff from the Bay of Bengal caused by the strengthened boreal summer monsoon in addition to increased local rainfall in the eastern equatorial Indian Ocean. Alternatively, during this period of strengthened ASM, the contributions of the relatively enriched south-easterly source to Tangga Cave may have been increased relative to the In-

dian Ocean contribution, resulting in a heavier than expected $\delta^{18}O$ value during the BA.

Cooler SSTs in the western Indian Ocean during the YD (Tierney et al., 2015), coupled with relatively constant SSTs in the eastern Indian Ocean (Mohtadi et al., 2014; Setiawan et al., 2015) could be used to infer a persistent negative Indian Ocean Dipole-like state (increased west–east SST gradient) in the Indian Ocean region during the YD. However, the reduced rainfall in the eastern Indian Ocean does not support a coupled increase in Indian and Pacific Walker Circulation, perhaps owing to the fact that the enhanced gradient is related to cooling anomalies in the western Indian Ocean, rather than warming in the eastern Indian Ocean. It could also signify that rainfall changes associated with weakening of the Asian and Indian monsoons dominate over any effects caused by the change in zonal SST gradients across the tropical Indian Ocean.

Indian Ocean hydroclimate does not mirror the zonal asymmetry observed in Indian Ocean SSTs. Idealized hosing experiments have been used to infer that a reorganization of Hadley circulation in the Indian Ocean, including a mean southward shift of the ITCZ and a weakening of the boreal summer monsoon, is a key response to North Atlantic freshwater forcing such as the YD (Lewis et al., 2011; Mohtadi et al., 2014). This interpretation is supported by proxy records from the western Indian Ocean, suggesting a zonally symmetric response in hydroclimate across the Indian Ocean during the YD. Speleothem records from Yemen indicate a reduction in the Indian Monsoon (Shakun et al., 2007), which considered with the Sumatran speleothem, demonstrates a widespread weakening across the entire Indian Ocean Basin. Both Lakes Challa (3°S) and Tanganyika (6°S) record isotopic enrichment across the YD (Tierney et al., 2008, 2011), while sites further south (Zambezi catchment (18°S), Lake Chilwa (15°S)) show isotopic depletion or lake level highstands (Schefuß et al., 2011; Thomas et al., 2009), likely signifying a southward shift in the ascending branch of the Hadley circulation.

The record from Sumatra supports a cross-basin YD response in Indian Ocean hydroclimate that is consistent with the signal observed in the ASM/ISM realm and in the offshore Sumatra $\delta^{18}O_{sw}$ reconstruction. Though records from Africa support a southward ITCZ shift, equatorial sites such as Tangga Cave should still be receiving rainfall from the ITCZ as it passes overhead at least once during its annual migration. Thus, a mean southwards ITCZ shift alone is unlikely to have caused the drying observed in Sumatra. Indeed, an examination of nearby proxies in the Indo-Pacific Warm Pool suggests a more complex mechanism.

4.3. The Younger Dryas in the Indo-Pacific Warm Pool

In the IPWP, a mean southward ITCZ shift during the YD has been inferred from amount-effect driven changes in $\delta^{18}O$ at sites on the meridional edges of the IPWP (Fig. 8). As with rainfall $\delta^{18}O$ in Sumatra, rainfall $\delta^{18}O$ at other IPWP sites may be controlled by a combination of moisture source and regional or local amount effect, with moisture source often enhancing the amount effect signal. The other IPWP sites have been interpreted in-line with each site's listed publication. These include an increase in precipitation recorded by speleothems from Flores (Ayliffe et al., 2013; Griffiths et al., 2009), and rainfall decreases in Palawan (Philippines) in the northern IPWP (Partin et al., 2015). The ^{18}O depletion over Flores during the YD contrasts with the YD ^{18}O enrichment in the Sumatran speleothem, suggesting that different processes dominated the YD hydroclimate response at the zonal and meridional margins of the IPWP.

Like China, the Palawan site in the northern IPWP receives the majority of its rainfall during the boreal summer monsoon season and shows a distinct decrease in rainfall during the YD (Partin et al., 2015). Models suggest that much of the northern IPWP dried out during boreal summer, with some simulations suggesting concurrent increases in precipitation in the austral tropics (Lewis et al., 2010) and others indicating no anomalous austral precipitation (Partin et al., 2015; Pausata et al., 2011). The former might indicate a southward position of the ITCZ during boreal summer. However, as the ITCZ still would have migrated north during boreal summer (McGee et al., 2014; Schneider et al., 2014) reaching the boreal tropics, drying in Palawan likely indicates a reduction of convective rainfall within the ITCZ during boreal summer or a reduction in the duration of the boreal summer season, rather than a southward shift.

In the southern part of the IPWP, Liang Luar Cave in Flores currently receives 70% of its rainfall during austral summer (December–March). During the YD, the Flores speleothem suggests a slight increase in rainfall, interpreted as an intensification of austral summer monsoon rainfall associated with a austral summer southward ITCZ shift (Griffiths et al., 2009). The YD signal is ambiguous in the precipitation record from northern Australia (Denniston et al., 2013), however, a precipitation increase at Flores and Ball Gown Cave during HS1 suggests a similar mechanism is at play (Ayliffe et al., 2013). It is possible that the austral summer ITCZ rain belt during the YD was shifted south relative to modern, but north relative to HS1, such that Flores received increased duration of rainfall, but not NW Australia.

To date, no YD response has been documented from equatorial sites from the IPWP. A speleothem record from Borneo (Partin et al., 2015) and a lake sediment leaf wax record from Sulawesi (Konecky et al., 2016) both show no clear rainfall response to the YD or BA. At 3°S, leaf wax from Lake Towuti, Sulawesi, suggests no change in rainfall during the austral summer monsoon (Konecky et al., 2016). Since both Flores and Sulawesi are biased towards the austral summer monsoon, it might be expected that intensified austral summer monsoon rainfall would manifest in the Sulawesi record during millennial-scale events. In contrast, if austral summer monsoon rainfall remained the same or decreased during the Younger Dryas, the ^{18}O depletion at Flores and neutral signal at Sulawesi must be attributed to either ITCZ duration overhead or latitudinal positioning. Flores, at the southern limit of modern ITCZ rainfall, might record increased rainfall due to its more prolonged duration under the ITCZ rain belt. Sulawesi may similarly be subject to an extended monsoon season, which may cancel out the reduction in moisture transport. Relative to Flores, which is only under the ITCZ during austral summer, Sulawesi, which is already under the ITCZ for a greater part of the year, may be less sensitive to an austral summer southward shift. Considered together, the records from Flores and Sulawesi suggest that ITCZ-related austral summer convective rainfall did not intensify, as this would result in an $\delta^{18}O$ decrease at both sites. Rather, the $\delta^{18}O$ signals at Flores and Sulawesi can be explained by changes in the duration of the ITCZ overhead associated with a southward ITCZ shift, without invoking an increase in convective rainfall.

If these assumptions are correct, then overall moisture transport along monsoon transport pathways during both boreal and austral summer was weaker or the same during the YD. Boreal summer monsoon rainfall reductions, like those observed at the Palawan site and across China and India, likely contribute to the Sumatra YD signal. However, because Sumatra also receives considerable rainfall contributions from other sources during the rest of the year, an increase in austral monsoon convective rainfall would be expected to counteract the boreal signal. However, the proxy evidence from the austral monsoon system does not necessitate an increase in moisture transport along the austral monsoon transport pathway.

Indeed, results from an idealized hosing experiment of the coupled ocean-atmosphere GISS ModelE-R (Lewis et al., 2010) sup-

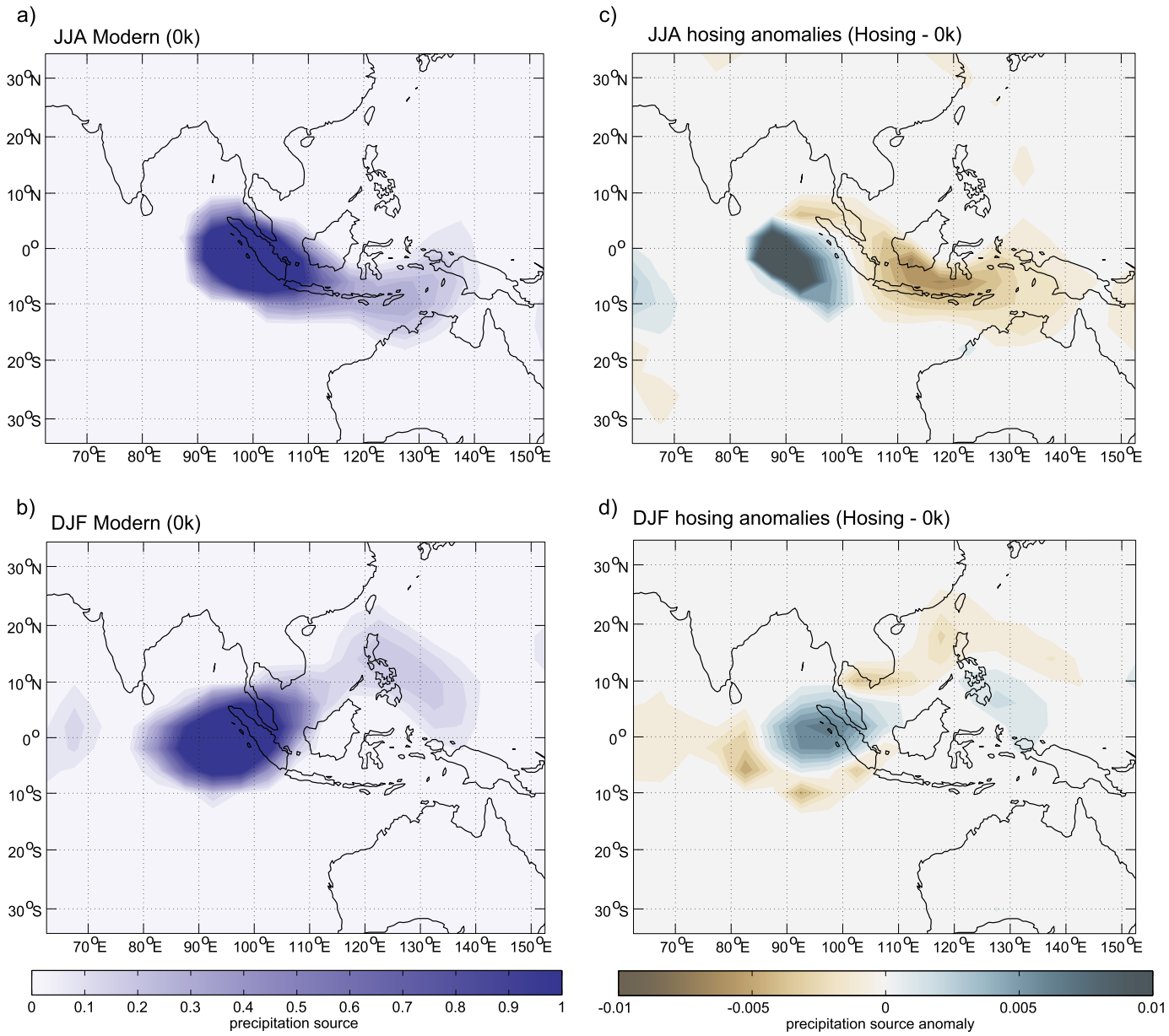

Fig. 9. GISS ModelE-R vapor source distribution (VSD) results for Tangga Cave, Sumatra. Modern (0k) precipitation source for a) JJA and b) DJF, and hosing precipitation source anomalies for c) JJA and d) DJF. The precipitation source distribution utilized in this study is a subset of the VSD, defined where vapor condenses to liquid. VSD resolution is $\sim 8 \times 10°$. VSDs are unitless probability density functions.

port the case for reduced monsoon-sourced rainfall to Sumatra. GISS ModelE-R is equipped with water vapor source distribution (VSD) tracers, which can be traced back through cloud processes to the site of surface evaporation. GISS ModelE-R VSD results indicate that both the austral and boreal monsoon moisture transport pathways for Tangga Cave (Fig. 3) were decreased relative to local Indian Ocean sources during hosing (Fig. 9). Though this implies an increase in the proportion of relatively ^{18}O-depleted Indian Ocean sources, the fact that Tangga Cave records ^{18}O enrichment suggests there must be a counteracting change in either the amount of rainfall from all sources or the transport distance, both of which would serve to increase δ^{18}O.

Reductions in the monsoon transport pathways do not preclude involvement of the Indian Ocean moisture source to the patterns observed in Sumatra. The Indian Ocean source can contribute to ^{18}O enrichment via a similar decrease in rainfall. Alternatively, or in concert with rainfall reduction, the Indian Ocean source becomes more localized, which could have resulted in less rainout along this transport path and more enriched isotopic values. A recent modeling study accurately captures the pattern of rainfall captured by IPWP proxies during HS1 (Mohtadi et al., 2014). During a freshwater hosing experiment, the simulation suggests that a strengthening of the Indian Ocean equatorial westerly winds would accompany a southward shift of the Indian Ocean Hadley cell, creating a strong subsidence anomaly above Sumatra.

If similar mechanisms were at play during the YD, these dry winds could punctuate eastward over Sumatra, but be constrained by the ascending branch of Pacific Walker circulation somewhere in the vicinity of Borneo. The speleothem record from Borneo (Partin et al., 2007) indicates no obvious rainfall anomaly during the YD. Today, the Borneo cave site receives rainfall year-round and is strongly influenced by Pacific climate variability associated with the El Niño-Southern Oscillation (ENSO) (Moerman et al., 2013; Partin et al., 2007). It has been suggested that Borneo may receive

opposing rainfall signals in summer and winter that canceled out a response to millennial scale ITCZ shifts during the YD (Partin et al., 2015). However, the Sumatra speleothem and GISS ModelE-R results indicate that net austral and boreal summer monsoon moisture transport are reduced, which should manifest as drying or enrichment at sites without a strong rainfall seasonality. An alternative is that the increasing precessional signal of boreal autumn insolation in the equatorial Pacific during the last glacial termination may dominate over North Atlantic forcing in the central Warm Pool during the YD, potentially explaining why no YD signal is observed despite the Borneo reconstruction containing multiple Heinrich events (Carolin et al., 2013, 2016; Partin et al., 2007).

Taken together, the proxy data from the Indo-Pacific Warm Pool suggest a reduction of moisture transport in both the austral and boreal monsoon transport pathways. Sites that exhibit a dry or ^{18}O-enriched YD (i.e., Palawan and Sumatra) are driven by weakening of summer monsoon transport. Sumatra may also be subject to reduced length of transport pathways during YD, leading to ^{18}O enrichment. Sites that demonstrate ^{18}O depletion interpreted as increased rainfall (i.e., Flores) observe an extended duration of the ITCZ overhead. Sites which show no response are very close to the equator and either highly seasonal (i.e. Sulawesi) such that the reduction of moisture transport may be counteracted by an increased season length, or overridden by other mechanisms that influence local precipitation, such as insolation (i.e., Borneo).

5. Conclusions

The new speleothem record from Sumatra demonstrates an extended spatial reach of the Younger Dryas climate anomaly into the eastern equatorial Indian Ocean region. This adds to previous evidence of a seawater δ^{18}O response offshore of Sumatra by confirming that the YD involved a rapid and marked ^{18}O enrichment of precipitation over central Sumatra and was not just an advected signal at nearby marine sites. The Sumatran speleothem record and VSD results indicate an overall weakening of moisture transport along both the boreal and austral monsoon transport pathways. This response does not preclude the involvement of a southward austral summer ITCZ shift and an Indian Ocean trade wind induced reduction of Indian Ocean-sourced rainfall. A signal of the YD climate anomaly appears at both the zonal and meridional edges of the IPWP, but is ambiguous in central IPWP records, potentially due to the overriding control of Pacific forcing during the last termination. Further isotope-enabled modeling studies will be useful to constrain the relative contributions of moisture source and amount effect, as well as further explore mechanisms that drive differences between the YD and HS1. The new speleothem record from Sumatra has important implications for the extent of North Atlantic forcing in the tropics, particularly in light of uncertainty about the future of Atlantic Meridional Overturning Circulation (Rahmstorf et al., 2015).

Acknowledgements

This research contributes to Australian Research Council (ARC) Discovery Project DP110101161 (led by Michael Gagan, and including Wahyoe Hantoro and NJA). We also thank the Research School of Earth Sciences, ARC Discovery Project DP140102059 (led by NJA) and the ARC Centre of Excellence for Climate System Science (CE110001028) for scholarship support awarded to JBW. NJA was supported by an ARC QEII fellowship (DP110101161), SCL by ARC DECRA Fellowship (160100092), and JCH by ARC Future Fellowship (FT130100801). Fieldwork was carried out under RISTEK permit 02/TKPIPA/FRP/SM/II/2012 with the endorsement of Wahyoe Hantoro and the Research Center for Geotechnology, Indonesian Institute of Sciences (LIPI). Fieldwork was funded by ARC Discovery Project DP110101161, and we thank Hamdi Rifai, Djupriano Djupri, Engkos Kosasih, Isnally Rifki, Claire Krause, and David Wools-Cobb for fieldwork assistance. We thank Joe Cali, Joan Cowley, Heather Scott-Gagan, Graham Mortimer, Stephen Eggins and Leslie Kinsley for valuable laboratory support of this study. We also thank Allegra LeGrande for her contributions to the GISS ModelE-R VSD analysis; Jodie Bradby and the Research School of Physics and Engineering (ANU) for access to and assistance with Raman spectroscopy; and Silvia Frisia for useful discussions that aided the research. We also thank the two anonymous reviewers whose comments improved this manuscript. The speleothem δ^{18}O and chronology data reported in this paper for Tangga Cave are archived at NOAA NCEI (https://www.ncdc.noaa.gov/paleo/study/23790).

References

Abram, N.J., Gagan, M.K., Cole, J.E., Hantoro, W.S., Mudelsee, M., 2008. Recent intensification of tropical climate variability in the Indian Ocean. Nat. Geosci. 1, 849–853. https://doi.org/10.1038/ngeo357.

Aldrian, E., Susanto, R.D., 2003. Identification of three dominant rainfall regions within Indonesia and their relationship to sea surface temperature. Int. J. Climatol. 23, 1435–1452. https://doi.org/10.1002/joc.950.

Ayliffe, L.K., Gagan, M.K., Zhao, J.-x., Drysdale, R.N., Hellstrom, J.C., Hantoro, W.S., Griffiths, M.L., Scott-Gagan, H., Pierre, E.S., Cowley, J.A., Suwargadi, B.W., 2013. Rapid interhemispheric climate links via the Australasian monsoon during the last deglaciation. Nat. Commun. 4, 2908. https://doi.org/10.1038/ncomms3908.

Bajo, P., Hellstrom, J., Frisia, S., Drysdale, R., Black, J., Woodhead, J., Borsato, A., Zanchetta, G., Wallace, M.W., Regattieri, E., Haese, R., 2016. "Cryptic" diagenesis and its implications for speleothem geochronologies. Quat. Sci. Rev. 148, 17–28. https://doi.org/10.1016/j.quascirev.2016.06.020.

Barker, S., Diz, P., Vautravers, M.J., Pike, J., Knorr, G., Hall, I.R., Broecker, W.S., 2009. Interhemispheric Atlantic seesaw response during the last deglaciation. Nature 457, 1097–1102. https://doi.org/10.1038/nature07770.

Belgaman, H.A., Ichiyanagi, K., Suwarman, R., Tanoue, M., Aldrian, E., Utami, A.I.D., Kusumaningtyas, S.D.A., 2017. Characteristics of seasonal precipitation isotope variability in Indonesia. Hydrol. Res. Lett. 11, 92–98. https://doi.org/10.3178/hrl.11.92.

Belgaman, H.A., Ichiyanagi, K., Tanoue, M., Suwarman, R., Yoshimura, K., Mori, S., Kurita, N., Yamanaka, M.D., Syamsudin, F., 2016. Intraseasonal variability of δ^{18}O of precipitation over the indonesian maritime continent related to the Madden–Julian oscillation. SOLA 12, 192–197. https://doi.org/10.2151/sola.2016-039.

Bintanja, R., van de Wal, R.S.W., Oerlemans, J., 2005. Modelled atmospheric temperatures and global sea levels over the past million years. Nature 437, 125–128. https://doi.org/10.1038/nature03975.

Blaauw, M., Christen, J.A., 2011. Flexible paleoclimate age-depth models using an autoregressive gamma process. Bayesian Anal. 6, 457–474. https://doi.org/10.1214/ba/1339616472.

Bond, G., Broecker, W., Johnsen, S., McManus, J., Labeyrie, L., Jouzel, J., Bonani, G., 1993. Correlations between climate records from North Atlantic sediments and Greenland ice. Nature 365, 143–147. https://doi.org/10.1038/365143a0.

Broecker, W.S., Denton, G.H., Edwards, R.L., Cheng, H., Alley, R.B., Putnam, A.E., 2010. Putting the Younger Dryas cold event into context. Quat. Sci. Rev. 29, 1078–1081. https://doi.org/10.1016/j.quascirev.2010.02.019.

Carolin, S.A., Cobb, K.M., Adkins, J.F., Clark, B., Conroy, J.L., Lejau, S., Malang, J., Tuen, A.A., 2013. Varied response of western Pacific hydrology to climate forcings over the last glacial period. Science 340, 1564–1566. https://doi.org/10.1126/science.1233797.

Carolin, S.A., Cobb, K.M., Lynch-Stieglitz, J., Moerman, J.W., Partin, J.W., Lejau, S., Malang, J., Clark, B., Tuen, A.A., Adkins, J.F., 2016. Northern Borneo stalagmite records reveal West Pacific hydroclimate across MIS 5 and 6. Earth Planet. Sci. Lett. 439, 182–193. https://doi.org/10.1016/j.epsl.2016.01.028.

Cheng, H., Lawrence Edwards, R., Shen, C.-C., Polyak, V.J., Asmerom, Y., Woodhead, J., Hellstrom, J.C., Wang, Y., Kong, X., Spötl, C., Wang, X., Calvin Alexander Jr., E., 2013. Improvements in ^{230}Th dating, ^{230}Th and ^{234}U half-life values, and U–Th isotopic measurements by multi-collector inductively coupled plasma mass spectrometry. Earth Planet. Sci. Lett. 371–372, 82–91. https://doi.org/10.1016/j.epsl.2013.04.006.

Chiang, J.C.H., Bitz, C.M., 2005. Influence of high latitude ice cover on the marine Intertropical Convergence Zone. Clim. Dyn. 25, 477–496. https://doi.org/10.1007/s00382-005-0040-5.

Dee, D.P., Uppala, S.M., Simmons, A.J., Berrisford, P., Poli, P., Kobayashi, S., Andrae, U., Balmaseda, M.A., Balsamo, G., Bauer, P., Bechtold, P., Beljaars, A.C.M., van de Berg, L., Bidlot, J., Bormann, N., Delsol, C., Dragani, R., Fuentes, M., Geer, A.J., Haimberger, L., Healy, S.B., Hersbach, H., Hólm, E.V., Isaksen, L., Kållberg, P., Köhler, M., Matricardi, M., McNally, A.P., Monge-Sanz, B.M., Morcrette, J.J., Park, B.K., Peubey, C., de Rosnay, P., Tavolato, C., Thépaut, J.N., Vitart, F., 2011. The ERA-Interim reanalysis: configuration and performance of the data assimilation system. Q. J. R. Meteorol. Soc. 137, 553–597. https://doi.org/10.1002/qj.828.

Denniston, R.F., Asmerom, Y., Lachniet, M., Polyak, V.J., Hope, P., An, N., Rodzinyak, K., Humphreys, W.F., 2013. A Last Glacial Maximum through middle Holocene stalagmite record of coastal Western Australia climate. Quat. Sci. Rev. 77, 101–112. https://doi.org/10.1016/j.quascirev.2013.07.002.

Denton, G.H., Anderson, R.F., Toggweiler, J.R., Edwards, R.L., Schaefer, J.M., Putnam, A.E., 2010. The last glacial termination. Science 328, 1652–1656. https://doi.org/10.1126/science.1184119.

Draxler, R.R., Hess, G.D., 1997. Description of the HYSPLIT_4 modeling system, NOAA Tech. Memo. ERL ARL-224. NOAA, Silver Spring, MD, p. 24.

Dutt, S., Gupta, A.K., Clemens, S.C., Cheng, H., Singh, R.K., Kathayat, G., Edwards, R.L., 2015. Abrupt changes in Indian summer monsoon strength during 33,800 to 5500 years B.P. Geophys. Res. Lett. 42, 5526–5532. https://doi.org/10.1002/2015GL064015.

Dykoski, C.A., Edwards, R.L., Cheng, H., Yuan, D., Cai, Y., Zhang, M., Lin, Y., Qing, J., An, Z., Revenaugh, J., 2005. A high-resolution, absolute-dated Holocene and deglacial Asian monsoon record from Dongge Cave, China. Earth Planet. Sci. Lett. 233, 71–86. https://doi.org/10.1016/j.epsl.2005.01.036.

Finch, A.A., Shaw, P.A., Weedon, G.P., Holmgren, K., 2001. Trace element variation in speleothem aragonite: potential for palaeoenvironmental reconstruction. Earth Planet. Sci. Lett. 186, 255–267. https://doi.org/10.1016/S0012-821X(01)00253-9.

Frisia, S., Borsato, A., Fairchild, I.J., McDermott, F., Selmo, E.M., 2002. Aragonite–calcite relationships in speleothems (Grotte De Clamouse, France): environment, fabrics, and carbonate geochemistry. J. Sediment. Res. 72, 687–699. https://doi.org/10.1306/020702720687.

Gibbons, F.T., Oppo, D.W., Mohtadi, M., Rosenthal, Y., Cheng, J., Liu, Z., Linsley, B.K., 2014. Deglacial δ^{18}O and hydrologic variability in the tropical Pacific and Indian Oceans. Earth Planet. Sci. Lett. 387, 240–251. https://doi.org/10.1016/j.epsl.2013.11.032.

Griffiths, M.L., Drysdale, R.N., Gagan, M.K., Zhao, J.-x., Ayliffe, L.K., Hellstrom, J.C., Hantoro, W.S., Frisia, S., Feng, Y.-X., Cartwright, I., Pierre E.J., St., Fischer, M.J., Suwargadi, B.W., 2009. Increasing Australian–Indonesian monsoon rainfall linked to early Holocene sea-level rise. Nat. Geosci. 2, 636–639. https://doi.org/10.1038/Ngeo605.

Heinrich, H., 1988. Origin and consequences of cyclic ice rafting in the Northeast Atlantic Ocean during the past 130,000 years. Quat. Res. 29, 142–152. https://doi.org/10.1016/0033-5894(88)90057-9.

Hellstrom, J., 2003. Rapid and accurate U/Th dating using parallel ion-counting multi-collector ICP-MS. J. Anal. At. Spectrom. 18, 1346–1351. https://doi.org/10.1039/B308781F.

Hellstrom, J.C., 2006. U–Th dating of speleothems with high initial ^{230}Th using stratigraphical constraint. Quat. Geochronol. 1, 289–295. https://doi.org/10.1016/j.quageo.2007.01.004.

Hughen, K.A., Overpeck, J.T., Peterson, L.C., Trumbore, S., 1996. Rapid climate changes in the tropical Atlantic region during the last deglaciation. Nature 380, 51–54. https://doi.org/10.1038/380051a0.

Kim, S.-T., O'Neil, J.R., Hillaire-Marcel, C., Mucci, A., 2007. Oxygen isotope fractionation between synthetic aragonite and water: influence of temperature and Mg^{2+} concentration. Geochim. Cosmochim. Acta 71, 4704–4715. https://doi.org/10.1016/j.gca.2007.04.019.

Knutti, R., Fluckiger, J., Stocker, T.F., Timmermann, A., 2004. Strong hemispheric coupling of glacial climate through freshwater discharge and ocean circulation. Nature 430, 851–856. https://doi.org/10.1038/nature02786.

Konecky, B., Russell, J., Bijaksana, S., 2016. Glacial aridity in central Indonesia coeval with intensified monsoon circulation. Earth Planet. Sci. Lett. 437, 15–24. https://doi.org/10.1016/j.epsl.2015.12.037.

Kurita, N., Ichiyanagi, K., Matsumoto, J., Yamanaka, M.D., 2009. The relationship between the isotopic content of precipitation and the precipitation amount in tropical regions. J. Geochem. Explor. 102, 113–122. https://doi.org/10.1016/j.gexplo.2009.03.002.

Lambeck, K., Rouby, H., Purcell, A., Sun, Y., Sambridge, M., 2014. Sea level and global ice volumes from the Last Glacial Maximum to the Holocene. Proc. Natl. Acad. Sci. USA. https://doi.org/10.1073/pnas.1411762111.

LeGrande, A.N., Schmidt, G.A., 2006. Global gridded data set of the oxygen isotopic composition in seawater. Geophys. Res. Lett. 33, L12604. https://doi.org/10.1029/2006GL026011.

Levi, C., Labeyrie, L., Bassinot, F., Guichard, F., Cortijo, E., Waelbroeck, C., Caillon, N., Duprat, J., de Garidel-Thoron, T., Elderfield, H., 2007. Low-latitude hydrological cycle and rapid climate changes during the last deglaciation. Geochem. Geophys. Geosyst. 8. https://doi.org/10.1029/2006GC001514.

Lewis, S.C., Gagan, M.K., Ayliffe, L.K., Zhao, J.-x., Hantoro, W.S., Treble, P.C., Hellstrom, J.C., LeGrande, A.N., Kelley, M., Schmidt, G.A., Suwargadi, B.W., 2011. High-resolution stalagmite reconstructions of Australian–Indonesian monsoon rainfall variability during Heinrich stadial 3 and Greenland interstadial 4. Earth Planet. Sci. Lett. 303, 133–142. https://doi.org/10.1016/j.epsl.2010.12.048.

Lewis, S.C., LeGrande, A.N., Kelley, M., Schmidt, G.A., 2010. Water vapour source impacts on oxygen isotope variability in tropical precipitation during Heinrich events. Clim. Past 6, 325–343. https://doi.org/10.5194/cp-6-325-2010.

Liebmann, B., Smith, C.A., 1996. Description of a complete (interpolated) outgoing longwave radiation dataset. Bull. Am. Meteorol. Soc. 77, 1275–1277.

Liu, Y., Henderson, G.M., Hu, C., Mason, A.J., Charnley, N.R., Johnson, K.R., Xie, S., 2013. Links between the East Asian monsoon and North Atlantic climate during the 8,200 year event. Nat. Geosci. 6, 117–120. https://doi.org/10.1038/ngeo1708.

Liu, Z., Wen, X., Brady, E.C., Otto-Bliesner, B., Yu, G., Lu, H., Cheng, H., Wang, Y., Zheng, W., Ding, Y., Edwards, R.L., Cheng, J., Liu, W., Yang, H., 2014. Chinese cave records and the East Asia Summer Monsoon. Q. Sci. Rev. 83, 115–128. https://doi.org/10.1016/j.quascirev.2013.10.021.

Marzin, C., Kallel, N., Kageyama, M., Duplessy, J.C., Braconnot, P., 2013. Glacial fluctuations of the Indian monsoon and their relationship with North Atlantic climate: new data and modelling experiments. Clim. Past 9, 2135–2151. https://doi.org/10.5194/cp-9-2135-2013.

McCulloch, M.T., Mortimer, G.E., 2008. Applications of the ^{238}U–^{230}Th decay series to dating of fossil and modern corals using MC-ICPMS. Aust. J. Earth Sci. 55, 955–965. https://doi.org/10.1080/08120090802097435.

McGee, D., Donohoe, A., Marshall, J., Ferreira, D., 2014. Changes in ITCZ location and cross-equatorial heat transport at the Last Glacial Maximum, Heinrich Stadial 1, and the mid-Holocene. Earth Planet. Sci. Lett. 390, 69–79. https://doi.org/10.1016/j.epsl.2013.12.043.

McLachlan, G., Peel, D., 2004. Finite Mixture Models. John Wiley & Sons.

McManus, J.F., Francois, R., Gherardi, J.-M., Keigwin, L.D., Brown-Leger, S., 2004. Collapse and rapid resumption of Atlantic meridional circulation linked to deglacial climate changes. Nature 428, 834–837. https://doi.org/10.1038/nature02494.

Moerman, J.W., Cobb, K.M., Adkins, J.F., Sodemann, H., Clark, B., Tuen, A.A., 2013. Diurnal to interannual rainfall δ^{18}O variations in northern Borneo driven by regional hydrology. Earth Planet. Sci. Lett. 369–370, 108–119. https://doi.org/10.1016/j.epsl.2013.03.014.

Mohtadi, M., Prange, M., Oppo, D.W., De Pol-Holz, R., Merkel, U., Zhang, X., Steinke, S., Luckge, A., 2014. North Atlantic forcing of tropical Indian Ocean climate. Nature 509, 76–80. https://doi.org/10.1038/nature13196.

Muller, J., Kylander, M., Wüst, R.A.J., Weiss, D., Martinez-Cortizas, A., LeGrande, A.N., Jennerjahn, T., Behling, H., Anderson, W.T., Jacobson, G., 2008. Possible evidence for wet Heinrich phases in tropical NE Australia: the Lynch's Crater deposit. Quat. Sci. Rev. 27, 468–475. https://doi.org/10.1016/J.Quascirev.2007.11.006.

NGRIP members, 2004. High-resolution record of Northern Hemisphere climate extending into the last interglacial period. Nature 431, 147–151. https://doi.org/10.1038/nature02805.

Partin, J.W., Cobb, K.M., Adkins, J.F., Clark, B., Fernandez, D.P., 2007. Millennial-scale trends in west Pacific warm pool hydrology since the Last Glacial Maximum. Nature 449, 452–455. https://doi.org/10.1038/Nature06164.

Partin, J.W., Quinn, T.M., Shen, C.C., Okumura, Y., Cardenas, M.B., Siringan, F.P., Banner, J.L., Lin, K., Hu, H.M., Taylor, F.W., 2015. Gradual onset and recovery of the Younger Dryas abrupt climate event in the tropics. Nat. Commun. 6, 8061. https://doi.org/10.1038/ncomms9061.

Pausata, F.S.R., Battisti, D.S., Nisancioglu, K.H., Bitz, C.M., 2011. Chinese stalagmite δ^{18}O controlled by changes in the Indian monsoon during a simulated Heinrich event. Nat. Geosci. 4, 474–480. https://doi.org/10.1038/ngeo1169.

Peterson, T.C., Vose, R.S., 1997. An overview of the Global Historical Climatology Network temperature database. Bull. Am. Meteorol. Soc. 78, 2837–2849. https://doi.org/10.1175/1520-0477(1997)078<2837:AOOTGH>2.0.CO;2.

Rahmstorf, S., Box, J.E., Feulner, G., Mann, M.E., Robinson, A., Rutherford, S., Schaffernicht, E.J., 2015. Exceptional twentieth-century slowdown in Atlantic Ocean overturning circulation. Nat. Clim. Change 5, 475–480. https://doi.org/10.1038/nclimate2554.

Rasmussen, S.O., Andersen, K.K., Svensson, A.M., Steffensen, J.P., Vinther, B.M., Clausen, H.B., Siggaard-Andersen, M.L., Johnsen, S.J., Larsen, L.B., Dahl-Jensen, D., Bigler, M., Röthlisberger, R., Fischer, H., Goto-Azuma, K., Hansson, M.E., Ruth, U., 2006. A new Greenland ice core chronology for the last glacial termination. J. Geophys. Res., Atmos. 111. https://doi.org/10.1029/2005jd006079.

Rosenthal, Y., Oppo, D.W., Linsley, B.K., 2003. The amplitude and phasing of climate change during the last deglaciation in the Sulu Sea, western equatorial Pacific. Geophys. Res. Lett. 30. https://doi.org/10.1029/2002GL016612.

Schefuß, E., Kuhlmann, H., Mollenhauer, G., Prange, M., Patzold, J., 2011. Forcing of wet phases in southeast Africa over the past 17,000 years. Nature 480, 509–512. https://doi.org/10.1038/nature10685.

Schneider, T., Bischoff, T., Haug, G.H., 2014. Migrations and dynamics of the intertropical convergence zone. Nature 513, 45–53. https://doi.org/10.1038/nature13636.

Schröder, J.F., Holbourn, A., Kuhnt, W., Küssner, K., 2016. Variations in sea surface hydrology in the southern Makassar Strait over the past 26 kyr. Quat. Sci. Rev. 154, 143–156. https://doi.org/10.1016/j.quascirev.2016.10.018.

Scroxton, N., 2014. Late Pleistocene Climate and Environment from Speleothems on Flores, Indonesia: Vegetation, Volcanoes and *Homo Floresiensis*. PhD Thesis, Research School of Earth Sciences, The Australian National University, p. 488.

Setiawan, R.Y., Mohtadi, M., Southon, J., Groeneveld, J., Steinke, S., Hebbeln, D., 2015. The consequences of opening the Sunda Strait on the hydrography of the eastern tropical Indian Ocean. Paleoceanography 30, 1358–1372. https://doi.org/10.1002/2015PA002802.

Shakun, J.D., Burns, S.J., Fleitmann, D., Kramers, J., Matter, A., Al-Subary, A., 2007. A high-resolution, absolute-dated deglacial speleothem record of Indian Ocean climate from Socotra Island, Yemen. Earth Planet. Sci. Lett. 259, 442–456. https://doi.org/10.1016/j.epsl.2007.05.004.

Sijinkumar, A.V., Clemens, S., Nath, B.N., Prell, W., Benshila, R., Lengaigne, M., 2016. $\delta^{18}O$ and salinity variability from the Last Glacial Maximum to Recent in the Bay of Bengal and Andaman Sea. Quat. Sci. Rev. 135, 79–91. https://doi.org/10.1016/j.quascirev.2016.01.022.

Sinha, A., Kathayat, G., Cheng, H., Breitenbach, S.F.M., Berkelhammer, M., Mudelsee, M., Biswas, J., Edwards, R.L., 2015. Trends and oscillations in the Indian summer monsoon rainfall over the last two millennia. Nat. Commun. 6. https://doi.org/10.1038/ncomms7309.

Steinke, S., Chiu, H.-Y., Yu, P.-S., Shen, C.-C., Erlenkeuser, H., Löwemark, L., Chen, M.-T., 2006. On the influence of sea level and monsoon climate on the southern South China Sea freshwater budget over the last 22,000 years. Quat. Sci. Rev. 25, 1475–1488. https://doi.org/10.1016/j.quascirev.2005.12.008.

Stott, L., Cannariato, K., Thunell, R., Haug, G.H., Koutavas, A., Lund, S., 2004. Decline of surface temperature and salinity in the western tropical Pacific Ocean in the Holocene epoch. Nature 431, 56–59. https://doi.org/10.1038/nature02903.

Stuiver, M., Grootes, P.M., 2000. GISP2 oxygen isotope ratios. Quat. Res. 53, 277–284. https://doi.org/10.1006/qres.2000.2127.

Suwarman, R., Ichiyanagi, K., Tanoue, M., Yoshimura, K., Mori, S., Yamanaka, M.D., Kurita, N., Syamsudin, F., 2013. The variability of stable isotopes and water origin of precipitation over the maritime continent. SOLA 9, 74–78. https://doi.org/10.2151/sola.2013-017.

Thomas, D.S.G., Bailey, R., Shaw, P.A., Durcan, J.A., Singarayer, J.S., 2009. Late Quaternary highstands at Lake Chilwa, Malawi: frequency, timing and possible forcing mechanisms in the last 44 ka. Quat. Sci. Rev. 28, 526–539. https://doi.org/10.1016/j.quascirev.2008.10.023.

Tierney, J.E., Pausata, F.S.R., deMenocal, P., 2015. Deglacial Indian monsoon failure and North Atlantic stadials linked by Indian Ocean surface cooling. Nat. Geosci. https://doi.org/10.1038/ngeo2603, advance online publication.

Tierney, J.E., Russell, J.M., Huang, Y., Damsté, J.S.S., Hopmans, E.C., Cohen, A.S., 2008. Northern hemisphere controls on tropical southeast African climate during the past 60,000 years. Science 322, 252–255. https://doi.org/10.1126/science.1160485.

Tierney, J.E., Russell, J.M., Sinninghe Damsté, J.S., Huang, Y., Verschuren, D., 2011. Late quaternary behavior of the East African monsoon and the importance of the Congo air boundary. Quat. Sci. Rev. 30, 798–807. https://doi.org/10.1016/j.quascirev.2011.01.017.

Vinther, B.M., Clausen, H.B., Johnsen, S.J., Rasmussen, S.O., Andersen, K.K., Buchardt, S.L., Dahl-Jensen, D., Seierstad, I.K., Siggaard-Andersen, M.L., Steffensen, J.P., Svensson, A., Olsen, J., Heinemeier, J., 2006. A synchronized dating of three Greenland ice cores throughout the Holocene. J. Geophys. Res., Atmos. 111. https://doi.org/10.1029/2005jd006921.

Waelbroeck, C., Kiefer, T., Dokken, T., Chen, M.T., Spero, H.J., Jung, S., Weinelt, M., Kucera, M., Paul, A., 2014. Constraints on surface seawater oxygen isotope change between the Last Glacial Maximum and the Late Holocene. Quat. Sci. Rev. 105, 102–111. https://doi.org/10.1016/j.quascirev.2014.09.020.

Wang, Y., Cheng, H., Edwards, R.L., An, Z., Wu, J., Shen, C.-C., Dorale, J.A., 2001. A high-resolution absolute-dated Late Pleistocene monsoon record from Hulu Cave, China. Science 294, 2345–2348. https://doi.org/10.1126/science.1064618.

White, W.B., 2006. Identification of cave minerals by Raman spectroscopy: new technology for non-destructive analysis. Int. J. Speleol. 35, 103–107. https://doi.org/10.5038/1827-806X.35.2.6.

Wilson, M.E.J., 2002. Cenozoic carbonates in Southeast Asia: implications for equatorial carbonate development. Sediment. Geol. 147, 295–428. https://doi.org/10.1016/S0037-0738(01)00228-7.

Xie, P., Arkin, P.A., 1997. Global precipitation: a 17-year monthly analysis based on gauge observations, satellite estimates, and numerical model outputs. Bull. Am. Meteorol. Soc. 78, 2539–2558. https://doi.org/10.1175/1520-0477(1997)078<2539:GPAYMA>2.0.CO;2.

Xu, J., Holbourn, A., Kuhnt, W., Jian, Z., Kawamura, H., 2008. Changes in the thermocline structure of the Indonesian outflow during Terminations I and II. Earth Planet. Sci. Lett. 273, 152–162. https://doi.org/10.1016/j.epsl.2008.06.029.

Yang, H., Johnson, K.R., Griffiths, M.L., Yoshimura, K., 2016. Interannual controls on oxygen isotope variability in Asian monsoon precipitation and implications for paleoclimate reconstructions. J. Geophys. Res., Atmos. https://doi.org/10.1002/2015JD024683.

Yoshimura, K., Kanamitsu, M., Noone, D., Oki, T., 2008. Historical isotope simulation using reanalysis atmospheric data. J. Geophys. Res., Atmos 113. https://doi.org/10.1029/2008JD010074.

Zhang, R., 2005. Simulated tropical response to a substantial weakening of the Atlantic thermohaline circulation.

Zhang, R., Delworth, T.L., 2005. Simulated tropical response to a substantial weakening of the Atlantic thermohaline circulation. J. Climate 18, 1853–1860. https://doi.org/10.1175/jcli3460.1.